Title: A Warm and Poorly Ventilated Deep Arctic Mediterranean During the Last Glacial

Authors: D.J.R. Thornalley[1,2*], H.A. Bauch,[3] G. Gebbie[1], W. Guo[1], M. Ziegler[4], S.M. Bernasconi[4], S. Barker[5], L.C. Skinner[6] & J. Yu[7].

Affiliations:

[1] Woods Hole Oceanographic Institution, Woods Hole, MA 02543, USA.

[2] Dept. Of Geography, University College London, London, UK.

[3] Mainz Academy c/o GEOMAR, Kiel, Germany.

[4] ETH Zurich, Switzerland.

[5] School of Earth and Ocean Sciences, Cardiff University, Cardiff, UK.

[6] Department of Earth Sciences, University of Cambridge, Cambridge, UK.

[7]Research School of Earth Sciences, Australian National University, Australia.

[*]Correspondence to: d.thornalley@cantab.net

Abstract: Changes in the formation of dense water in the Arctic Ocean and Nordic Seas (the ôArctic Mediterraneanõ, AM) likely contributed to the altered climate of the last glacial period. We examine past changes in AM circulation by reconstructing ^{14}C ventilation ages of the deep Nordic Seas over the last 30,000 years. Our results show that the deep glacial AM was extremely poorly ventilated (ventilation ages of up to 10,000 years). Subsequent episodic overflow of aged water into the mid-depth North Atlantic occurred during deglaciation. Proxy data also suggest the deep glacial AM was ~2-3°C warmer than modern; deglacial mixing of the deep AM with the upper ocean thus potentially contributed to melting sea-ice and icebergs, as well as proximal terminal ice-sheet margins.

One Sentence Summary: New proxy data reveals the extremely poor ventilation of a warmer, glacial deep Arctic Mediterranean, which overflowed into the Northeast Atlantic during the last deglaciation.

Main Text: The Atlantic meridional overturning circulation (AMOC) plays an important role in Earthôs climate because it redistributes ocean heat and helps control the storage of carbon in the deep ocean. The primary northern hemisphere sources of dense water supplied to the AMOC are produced in the Arctic Mediterranean (*1*). Here, warm surface waters from the Atlantic flow northwards and circulate around the AM via several different pathways, gradually cooling, thereby releasing heat to the atmosphere, and becoming denser. Much of this water mass transformation is thought to occur in the Nordic Seas via intermediate and deep open ocean convection, with a smaller contribution from the Arctic that also involves the addition of dense waters from brine-enhanced shelf water production (*1, 2*). The dense water produced by these

processes overflows the Greenland-Scotland Ridge (GSR), ultimately forming lower North Atlantic Deep Water (NADW), as part of the deep southward return flow of the AMOC.

Because of the northward heat transfer associated with the flow of warm surface water to convection sites, changes in deep water formation in the North Atlantic and Nordic Seas are thought to be associated with the altered climate of the last glacial maximum (LGM) and the abrupt climate events of the last deglaciation (~19 to 7 thousand years ago, ka), such as the northern hemisphere cold intervals Heinrich Stadial 1 (HS1) and the Younger Dryas (YD) (*3-5*), which affected global climate (*6, 7*). In this study we investigate circulation changes over the past 30 ka in the deep Norwegian Sea (and by inference, the broader AM) by reconstructing radiocarbon ventilation age and deep ocean temperature. Our results reveal an absence of deep convection within the AM throughout much of the last glacial and deglaciation and instead suggest the presence of a relatively warm and extremely poorly ventilated water mass in the glacial deep AM that subsequently overflowed southward into the North Atlantic during the deglaciation.

North Atlantic radiocarbon reconstructions. Several studies have utilised seawater radiocarbon ratios ($\Delta^{14}C$) as a proxy for investigating past changes in the circulation of the North Atlantic, e.g. (*8-12*). In the modern high latitude North Atlantic, deep convection in the Nordic Seas and Labrador Seas quickly transfers to depth surface waters that have equilibrated with the atmosphere, resulting in a minimal surface-to-deep gradient in ^{14}C age (~100 years) (*13*) and well ventilated deep water in the North Atlantic.

Deglacial $\Delta^{14}C$ reconstructions from the subtropical North Atlantic are consistent with the established view that there was shoaling of the AMOC (involving a switch from NADW formation to Glacial North Atlantic Intermediate Water, GNAIW) and a northward incursion into the deep North Atlantic of more ^{14}C- depleted southern sourced water (SSW) (*8, 11*) during the last glacial, HS1 and the YD. However, these data also reveal that large fluctuations in $\Delta^{14}C$ (shifts of up to ~1000 ^{14}C years within ~100 calendar years) occurred at mid-depths during HS1 and the YD, suggesting a complex history of mid-depth circulation (*8*). Recently, these fluctuations in mid-depth $\Delta^{14}C$, alongside temperature proxy data, have been used to propose a mechanism by which the AMOC switched from a glacial to interglacial mode of circulation through the release of heat from warm deep water (*14*).

$\Delta^{14}C$ reconstructions from the mid-depth (1.2-2.3 km) subpolar Northeast Atlantic, south of Iceland, have revealed the presence of an extremely poorly ventilated water mass during cold intervals of the last deglaciation, with ^{14}C ventilation ages in excess of 5000 years (*12*). Not only are the ventilation ages themselves striking, but also noteworthy are the rapid and large fluctuations that occurred within HS1 and the YD. These are similar to the variability reconstructed in the subtropical Northwest Atlantic although the shifts south of Iceland are up to four times larger in amplitude. The source of the poorly ventilated water south of Iceland was initially interpreted as Antarctic Intermediate Water (AAIW) (*12*), but more recent studies have since shown that AAIW in the deglacial Atlantic was not as poorly ventilated as the water south of Iceland (*9, 15, 16*). Available evidence also suggests that deep SSW was not sufficiently depleted in ^{14}C to explain the South Iceland Rise data (*8-10*) nor can it explain the distinct $\delta^{13}C$-$\Delta^{14}C$ relationship observed south of Iceland (*12*). An alternative proposed source is the AM, although so far there are no existing ^{14}C ventilation data from the deep AM to test this hypothesis. Reconstructions of ^{14}C ventilation ages from the shallow (~700 m) Iceland Sea

during the last glacial reveal benthic ventilation ages of ~500 years, indicating a well ventilated intermediate depth Nordic Seas that may have contributed to GNAIW (*3, 17*).

This study is therefore motivated by two aims: Firstly, to increase our understanding of the circulation of the AM and to investigate whether there was continued deep convection in the Nordic Seas (or AM as a whole) during the last glacial. It is important to better constrain past circulation changes in the AM because: (i) the amount of exchange between the surface and deep AM alters the properties of the exported dense water from the AM (*1, 2*); (ii) regional and global climate are directly influenced by the northward heat transport associated with the inflow of warm surface waters feeding the high latitude dense water formation sites (*2*), and (iii) ocean circulation changes have the potential to impact other components of the climate system, such as sea-ice extent and circum-AM ice sheets. We also wish to investigate the cause of the mid-depth radiocarbon anomalies recorded south of Iceland. The present lack of a viable explanation for the South Iceland Rise data suggest a knowledge gap in our understanding of deglacial ocean circulation. Moreover, a more complete interpretation of deglacial variability in mid-depth North Atlantic ^{14}C-ventilation ages, which, for example, has been examined in recent studies from the New England seamounts (*14, 18*), first requires us to constrain the various end-member water masses and the mechanisms by which they formed.

Ventilation changes in the AM. We have obtained new benthic and planktic radiocarbon measurements from a marine sediment core located in the Norwegian Sea (PS1243, 2.7 km depth, Fig. 1), selected because of its well defined stratigraphy (*19*). The age model has been slightly modified from its original planktic ^{14}C based chronology by tuning planktic δ^{18}O to nearby cores that themselves have been placed on a Greenland ice core based age model (see Fig. 2 and Supporting Online Materials and Methods, SOM). Core sites from within the central Arctic were not chosen because of the low abundance of benthic foraminifera, and the extremely low glacial sedimentation rate (*20*) would further increase the uncertainty in the stratigraphic age of samples, and hence the reconstruction of Δ^{14}C.

Table 1 and Fig. 2 show that, in contrast to the well ventilated deep waters and small benthic-planktic (B-P) ^{14}C offset (~100 years) of the Holocene and present day, much of the late glacial and deglacial Norwegian Sea was characterized by extremely poorly ventilated deep waters, with benthic ventilation ages of ~7000-10,000 years (and B-P ^{14}C offsets of a similar magnitude). Moreover, these extremely old ventilation ages are only associated with a modest decrease in benthic δ^{13}C values. The coupling of relatively high δ^{13}C values (~0.8-1.4ă) with extremely old ^{14}C ventilation ages suggests that the aging of deep waters was not accompanied by substantial remineralization of organic matter at depth, probably reflecting low surface productivity (Fig. 3 and SOM). These data further suggest that the deep Norwegian Sea was the likely source of poorly ventilated water south of Iceland during the deglaciation (*12*), and the slightly lower δ^{13}C reconstructed south of Iceland during deglacial cold intervals can be explained by mixing between the Nordic overflow and low-δ^{13}C SSW (Fig. 3). The observation of a poorly ventilated, yet high δ^{13}C endmember highlights the complexity of interpreting benthic δ^{13}C in the subpolar Northeast Atlantic which cannot simply be interpreted as a simple two end-member mixing scenario (i.e. SSW vs. GNAIW/NADW). Our results demonstrate that during the deglaciation, we must consider an extremely poorly ventilated Nordic Seas overflow with δ^{13}C of ~0.8-1.4ă , whilst earlier, during the LGM, the chemically distinct contribution to GNAIW identified by ref. (*21*) must have been sourced from the intermediate (not deep) Nordic Seas. The high δ^{13}C of both the *Cibicidoides wuellerstorfi* at this site and from the benthic foraminifera samples used for

$\Delta^{14}C$ (Table S1) rule out low $\delta^{13}C$ sources of ^{14}C-depleted carbon such as methane hydrates, mantle carbon or remineralized sedimentary organic carbon.

Our records indicate enhanced ventilation at the onset of the Holocene and the Bølling-Allerød (B-A; although additional measurements are ideally required for confirmation ï see SOM), as well as an event at ~16 ka, that is in agreement with measurements from south of Iceland. Support for the existence of a brief (multi-centennial scale or less) deep water formation event at ~16 ka, with a benthic-atmosphere offset of ~300 years recorded both in the deep Norwegian Sea at 2.7 km depth, and south of Iceland at 2.3 km depth (*12*), can also be found from high resolution planktic foraminifer faunal assemblage records in the subpolar Northeast Atlantic (SOM, Fig. S3), which reveal a strong surface warming recorded further south, possibly caused by an increased northward flow of surface waters feeding the deep convection site, the precise location of which is uncertain.

Isolation of the deep central Arctic. The magnitude and rapidity of the shift from well-ventilated to poorly-ventilated water at ~23 ka cannot be explained by *in situ* aging of deep water at the Norwegian Sea core site; therefore, we infer the incursion of a pre-aged, water mass. The most likely candidate for this is shoaling of isolated water in the deep central Arctic Ocean (see SOM), connected to the Nordic Seas via Fram Strait, with a volume of ~1.2 x 10^7 km^3 below 1 km water depth (*22*), approximately four times greater than the deep (>1 km) Nordic Seas. Because the Arctic Ocean (and AM as a whole) is a semi-enclosed basin, that was further restricted during the last glacial with the closure of the Bering Strait, it was susceptible to isolation and the development of a poorly ventilated water mass.

Previous studies have suggested that there was thick ice-cover across much of the Arctic during the last glacial maximum, leading to minimal or no sedimentation in the central Arctic of either terrigenous or biogenic material (*20, 23*). With no appreciable surrounding continental shelf area there was probably also only a minor contribution to the deep from brine-enhanced shelf water (*24*). These conditions would favor the development of poorly ventilated bottom water with relatively high $\delta^{13}C$. Benthic $\delta^{13}C$ data from the deep central Arctic prior to the last glacial (i.e. Marine Isotope Stage (MIS) 3) suggest values of up to 1.7-1.8ă (*25*), allowing for a small amount of remineralisation of organic carbon to have occurred throughout the glacial (MIS 2), resulting in the observed glacial and deglacial values in the deep Nordic Seas of 0.8-1.4ă . Reduced surface productivity across much of the glacial AM and organic carbon export to the North Atlantic by vigorous intermediate depth circulation presumably also helped prevent the development of anoxia in the deep AM (see SOM).

Projecting back the benthic $\Delta^{14}C$ onto the atmosphere $\Delta^{14}C$ curve (e.g. (*11*) and Fig. 2) for the data point at ~23 ka (i.e. the first occurrence of old water at PS1243), using a 400 years surface reservoir age, suggests that the deep Arctic Ocean may have become ásolatedô at ~30 ka, i.e. close to the onset of MIS 2, when sea-level records indicate the final rapid growth of continental ice-sheets to their full glacial extent (*26*) and hence the loss of shelf seas, reducing vertical mixing (*27*) and brine-enhanced shelf water production (*24*). However, this method does not consider any mixing and entrainment with younger waters, therefore if such entrainment occurred, it is possible that parts of the AM were older than our recorded ages and the deep central AM was isolated early than ~30 ka. Given its complex bathymetry, it is plausible that there were numerous distinct water masses residing within the deep AM during the last glacial, with various ventilation ages and nutrient chemistry.

Circulation changes and rates. Deep open ocean convection in the Nordic Seas is delicately poised today (*28*); therefore it seems probable that during the late glacial and deglacial, enhanced surface freshening caused the weakening and shoaling of open ocean convection in the Nordic Seas, so that the deep AM was only ventilated by limited deep water formation, likely in coastal polynyas. The timing of the switch to poorly ventilated waters at ~23 ka in the deep Norwegian Sea may have been the result of a marked weakening/shoaling of deep convection in response to surface freshening from melting ice-bergs (*19*), or alternatively, it was simply due to the slow accumulation and filling of the AM by bottom water which was denser than the products of Nordic Seas open ocean convection. Thus, the rapid switch to older benthic ventilation ages in PS1243 at ~23 ka likely records the upward migration of a sharp vertical gradient in radiocarbon ventilation age separating the aged AM bottom waters from the overlying, better ventilated, products of open ocean convection (see SOM), somewhat analogous to the situation invoked for the glacial Atlantic Ocean, with dense SSW, formed partly by brine rejection processes around Antarctica, being overlain by well-ventilated GNAIW - the product of open ocean convection south of Iceland (*29*). The mechanism by which the aged water mass was then transported into the North Atlantic is uncertain, but must have involved either the continued slow accumulation of aged water in the AM and its eventual overflow into the North Atlantic, or alternatively a more rapid process of entrainment and displacement by overturning in the Nordic Seas during the deglaciation, possibly related to sea-ice formation and brine rejection as orbitally induced insolation changes promoted summer melting of sea-ice and refreezing during winter. Investigating these mechanisms will require a depth transect of cores to reconstruct water column $\Delta^{14}C$ profiles at time intervals throughout the glacial and early deglacial.

If the deep ventilation age of 10,000 years is interpreted as a water mass residence time of ~10,000 years in the deep AM, then we can infer that the replenishment rate of deep water must have been limited to ~0.05 Sv, presumably by processes such as brine-enhanced dense water production in coastal polynyas. This rate can be compared to estimates of ~0.1 Sv for the modern contribution of brine-enhanced shelf-slope and entrained water into the deep Canadian Basin (*30*). Employing estimates of vertical diffusivity from the modern Arctic in a simple advective-diffusive model of the deep Arctic demonstrates that ventilation ages similar to those that we reconstruct in the glacial deep AM (~10,000 years) are achievable, as long as bottom water formation rates remain small (see SOM).

Recent work has suggested that there was persistent export of ^{231}Pa from the deep central Arctic Ocean over the past 35 ka (*31*). A likely sink for the ^{231}Pa was suggested to be the Fram Strait, where particle fluxes were higher, enabling scavenging of dissolved ^{231}Pa to the seafloor (*32*). To reconcile this with our results, we must infer that there was sufficient recirculation of the poorly ventilated deep water within the AM to enable the export of dissolved ^{231}Pa to Fram Strait. However, because uncertainties also remain regarding the influence of reduced glacial particle-rain and boundary scavenging on the glacial Arctic ^{231}Pa budget, these factors may also be called upon to explain the glacial Arctic ^{231}Pa deficit (*31*).

Implications. Using simple mass balance calculations regarding the possible volume of the poorly ventilated reservoir (i.e. that of the deep AM), limitations on its renewal rate (~0.05 Sv), and the observations from south of Iceland indicating overflow for a total of ~5000 years (i.e., the combined duration of HS1, YD and Intra-Allerød Cold Period, when highly ^{14}C depleted water is recorded in the overflow region (*12*)), the overflow of poorly ventilated waters from the AM into the Northeast Atlantic must have been relatively weak, and would not have exceeded,

on average, ~0.1 Sv. Future modelling work, aided by more proxy reconstructions, should investigate whether the mid-depth $\Delta^{14}C$ variability reconstructed in the subtropical Northwest Atlantic (*8*) can be attributed to a weak yet highly ^{14}C-depleted Nordic Seas overflow (*18*), and how this signal propagated throughout the North Atlantic under reduced AMOC conditions. Possibly the AM was the source for the low $\Delta^{14}C$ event at 15.6 ka recorded at the New England seamounts (*14, 18*). However the reconstructed temperatures of the deglacial AM (discussed later) are colder than the reconstructed temperatures at the New England seamounts for the 15.6 ka event (~0-1°C *vs.* 3-4°C), therefore substantial mixing with a warmer water mass must also have occurred.

The evidence for a poorly ventilated deep Nordic Seas also enables us to conclude that there was no significant contribution from the deep Nordic Seas (and by inference also the deep Arctic Ocean) to the formation of GNAIW. This contrasts with suggestions by earlier workers (*33*) which relied solely on benthic $\delta^{13}C$. Given faunal evidence for a persistent Atlantic inflow into the Nordic Seas (*34*) and possibly as a subsurface layer into the Arctic (*35*), shallow/intermediate overturning in the Nordic Seas likely persisted throughout the LGM, contributing to GNAIW, as suggested by previous studies (*3, 17, 19, 21, 36*). We also draw attention to the implication that, while the deep AM remained isolated from the overlying, better-ventilated upper ocean, any surface inputs/perturbations to the AM, such as meltwater events, would not have mixed throughout the entire basin, rather, they would have largely been confined to the upper ocean.

A warm, glacial deep AM. Because of deep convection, the modern deep Nordic Seas have a temperature of approximately -1 to -1.5°C. Published temperature proxy data, using ostracod Mg/Ca ratios from core PS1243, indicate that glacial temperatures of the deep Norwegian Sea were ~2-3°C warmer than during the Holocene (*35*). In support of the warming inferred from the ostracod Mg/Ca data, newly obtained clumped isotope and Mg/Ca temperature proxy data measured on benthic foraminifera in PS1243 and neighbouring core MD992276 indicate that the LGM was 2.9±1.5°C and 3.0±1.0°C warmer than the Holocene, respectively, in agreement with the ostracod temperature estimates (Fig. 5 and SOM). A 2-4°C warmer-than-modern, intermediate-to-deep AM has been inferred during MIS 3, caused by a deep inflow of Atlantic water (*24, 35*). During MIS 2, when we infer an isolated deep AM, it is likely that geothermal heating contributed to warming the deep AM. Geothermal heating is 40ï 60 mW m^{-2} for the modern Arctic (*37*), and assuming all the geothermal heat remained in a bottom water layer 2000m thick, the bottom water could warm by ~2°C over 10 kyr.

Because of the thermobaric effect, the development of warm and presumably relatively salty deep water, when overlain by colder and fresher water, provides a source of potential energy that can help drive ocean mixing and overturning (*38*). Overturning of the deep Nordic Seas (or Arctic) would allow the release of heat previously stored in the deep ocean, which could promote the melting of sea-ice and destabilise marine-terminating ice sheets, such as the Barents Sea ice-shelf, contributing to the deglaciation of the region. Ostracod Mg/Ca (*35*) and our new benthic foraminifera Mg/Ca data from the Norwegian Sea suggest that much of the heat stored in the deep Nordic Seas was released over the interval ~18-15 ka, i.e. during the early deglacial, centred around HS1 (Fig. 5). If deep AM waters were brought to the surface ocean, their carbon isotope composition must not have re-equilibrated with the atmosphere since old ventilation ages are still recorded during the YD, when the deep AM appears to have lost much of its glacial heat. Likely this was due to surface stratification, sea-ice cover and insufficient time at the surface for equilibration (analogous to modern upwelling Circumpolar Deep Water and Antarctic Bottom

Water formation). Whereas previous studies have suggested that a hypothesized subsurface incursion of warm Atlantic water during HS1 triggered the collapse of ice-shelves (*39*), we speculate that the release of deep ocean heat stored in the previously isolated deep AM may have also contributed to the melting of ice-shelves and terminal ice-sheet margins (as well as sea-ice and icebergs) in the circum-AM during the glacial termination. Plausibly, the build-up and release of heat from a glacial, isolated, deep AM also played a role in earlier terminations.

References and Notes

1. K. Aagaard, J. H. Swift, E. C. Carmck, *Journal of Geophysical Reasearch* **90**, 4833-4846 (1985).
2. C. Mauritzen, *Deep Sea Research* **43**, 769-806 (1996).
3. M. Sarnthein *et al.*, in *Northern North Atlantic: A Changing Environment,* P. R. Schafer, W.; Schluter, W.; Thiede, J., Ed. (Springer, Berlin, 2001), pp. 365-410.
4. S. Rahmstorf, *Nature* **419**, 207-214 (2002).
5. T. Dokken, E. Jansen, *Nature* **401**, 458-461 (1999).
6. S. Barker *et al.*, *Nature* **457**, 1097-1101 (2009).
7. J. D. Shakun *et al.*, *Nature* **484**, 49-54 (2012).
8. L. F. Robinson *et al.*, *Science* **310**, 1469-1473 (2005).
9. A. Burke, L. F. Robinson, *Science* **335**, 557-561 (2012).
10. L. C. Skinner, S. Fallon, C. Waelbroeck, E. Michel, S. Barker, *Science* **328**, 1147-1151 (2010).
11. L. C. Skinner, N. J. Shackleton, *Paleoceanography* **19**, Pa2005 Artn pa2005 (2004).
12. D. J. R. Thornalley, S. Barker, W. Broecker, H. Elderfield, I. N. McCave, *Science* **331**, 202-205 (2011).
13. W. Broecker, T. H. Peng, *Tracers in the Sea*. (Lamont Doherty Geological Observatory, 1982), pp. 690pp.
14. N. Thiagarajan, A. V. Subhas, J. R. Southon, J. M. Eiler, J. F. Adkins, *Nature* **511**, 75-78 (2014).
15. C. Cleroux, P. deMenocal, T. Guilderson, *Quaternary Science Reviews* **30**, 1875-1882 (2011).
16. R. N. Sortor, D. C. Lund, *Earth and Planetary Science Letters* **310**, 65-72 (2011).
17. M. Sarnthein, P. Grootes, J. P. Kennett, M. J. Nadeau, in *Ocean Circulation: Mechanisms and Impacts,* A. Schmittner, J. Chang, S. Hemming, Eds. (AGU Monograph Series, 2007), vol. 173.
18. D. J. Wilson, K. C. Crocket, T. v. d. Flierdt, L. F. Robinson, J. F. Adkins, *Paleoceanography* **29**, doi:10.1002/2014PA002674 (2014).
19. H. A. Bauch *et al.*, *Quaternary Science Reviews* **20**, 659-678 (2001).
20. L. Polyak *et al.*, *Global and Planetary Change* **68**, 5-17 (2009).
21. J. Yu, H. Elderfield, A. M. Piotrowski, *Earth and Planetary Science Letters* **271**, 209-220 (2008).
22. M. Jakobsson, *Geochemistry Geophysics Geosystems* **3**, 10.1029/2001gc000302 (2002).
23. R. F. Spielhagen, *Polarforschung* **82**, 19-36 (2012).
24. D. Bauch, H. A. Bauch, *Journal of Geophysical Research-Oceans* **106**, 9135-9143 (2001).
25. R. Stein *et al.*, *Science* **264**, 692-696 (1994).
26. P. U. Clark *et al.*, *Science* **325**, 710-714 (2009).
27. T. P. Rippeth *et al.*, *Nature Geosci* **8**, 191-194 (2015).

28. R. L. Dickson, J.; Meinicke, J; Rhines, P.; Swift, P., *Progr. Oceanogr.* **38**, 241-295 (1996).
29. W. B. Curry, D. Oppo, *Paleoceanography* **20**, PA1017, doi:1010.1029/2004PA001021 (2005).
30. E. P. Jones, B. Rudels, L. G. Anderson, *Deep-Sea Research Part I-Oceanographic Research Papers* **42**, 737-760 (1995).
31. S. S. Hoffmann, J. F. McManus, W. B. Curry, L. S. Brown-Leger, *Nature* **497**, 603-606 (2013).
32. N. Norgaard-Pedersen *et al.*, *Paleoceanography* **18**, 10.1029/2002PA000781 (2003).
33. T. Veum, E. Jansen, M. Arnold, I. Beyer, J.-C. Duplessey, *Nature* **356**, 783-785 (1992).
34. U. Pflaumann *et al.*, *Paleoceanography* **18**, 10.1029/2002PA000774 (2003).
35. T. M. Cronin *et al.*, *Nature Geoscience* **5**, 631-634 (2012).
36. M. Y. Meland, T. M. Dokken, E. Jansen, K. Hevroy, *Paleoceanography* **23**, 10.1029/2007PA001416 (2008).
37. M. L. Timmermans, C. Garrett, E. Carmack, *Deep-Sea Research Part I-Oceanographic Research Papers* **50**, 1305-1321 (2003).
38. J. F. Adkins, A. P. Ingersoll, C. Pasquero, *Quaternary Science Reviews* **24**, 581-594 10.1016/j.quascirev.2004.11.005 (2005).
39. S. A. Marcott *et al.*, *Proceedings of the National Academy of Sciences of the United States of America* **108**, 13415-13419 (2011).
40. P. J. Reimer *et al.*, *Radiocarbon* **51**, 1111-1150 (2009).
41. T. L. Rasmussen, E. Thomsen, *Geophysical Research Letters* **36**, 10.1029/2008gl036563 (2009).
42. C. H. Lear, E. M. Mawbey, Y. Rosenthal, *Paleoceanography* **25**, 10.1029/2009pa001880 (2010).
43. A. K. Tripati *et al.*, *Geochimica Et Cosmochimica Acta* **74**, 5697-5717 (2010).
44. P. Schlosser *et al.*, *Nuclear Instruments & Methods in Physics Research Section B-Beam Interactions with Materials and Atoms* **123**, 431-437 (1997).
45. T. M. Dokken, K. H. Nisancioglu, C. Li, D. S. Battisti, C. Kissel, *Paleoceanography* **28**, 491-502 (2013).
46. S. Barker, M. Greaves, H. Elderfield, *Geochemistry, Geophysics, Geosystems* **4**, doi:10.1029/2003GC000559 (2003).
47. K. J. Dennis, H. P. Affek, B. H. Passey, D. P. Schrag, J. M. Eiler, *Geochimica Et Cosmochimica Acta* **75**, 7117-7131 (2011).
48. B. H. Passey, N. E. Levin, T. E. Cerling, F. H. Brown, J. M. Eiler, *Proceedings of the National Academy of Sciences of the United States of America* **107**, 11245-11249 (2010).
49. G. A. Henkes *et al.*, *Geochimica Et Cosmochimica Acta* **106**, 307-325 (2013).
50. T. W. Schmid, S. M. Bernasconi, *Rapid Communications in Mass Spectrometry* **24**, 1955-1963 (2010).
51. T. W. Schmid, J. Radke, S. M. Bernasconi, *Thermo Fisher Application Note* 30233 (2012).
52. S. M. Bernasconi *et al.*, *Rapid Communications in Mass Spectrometry* **27**, 603-612 (2013).
53. A. N. Meckler, M. Ziegler, M. I. Millan, S. F. M. Breitenbach, S. M. Bernasconi, *Rapid Communications in Mass Spectrometry* **28**, 1705-1715 (2014).

54. S. Zaarur, H. P. Affek, M. T. Brandon, *Earth and Planetary Science Letters* **382**, 47-57 (2013).
55. W. Guo, J. L. Mosenfelder, W. A. Goddard, III, J. M. Eiler, *Geochimica Et Cosmochimica Acta* **73**, 7203-7225 (2009).
56. E. A. Schauble, P. Ghosh, J. M. Eiler, *Geochimica Et Cosmochimica Acta* **70**, 2510-2529 (2006).
57. P. Ghosh *et al.*, *Geochimica Et Cosmochimica Acta* **70**, 1439-1456 (2006).
58. R. A. Eagle *et al.*, *Biogeosciences* **10**, 4591-4606 (2013).
59. K. J. Dennis, D. P. Schrag, *Geochimica Et Cosmochimica Acta* **74**, 4110-4122 (2010).
60. J. Swift *et al.*, *Deep-Sea Res. II* **44**, 1503-1529 (1997).
61. R. Schlitzer, *Geophysical Monograph* **114**, 107-124 (2000).
62. D. Hebbeln, T. Dokken, E. Andersen, M. Hald, A. Elverhoi, *Nature* **370**, 357-360 (1994).
63. A. L. Magana *et al.*, *Paleoceanography* **25**, 10.1029/2010pa002011 (2010).
64. I. M. Lagerklint, J. D. Wright, *Geology* **27**, 1099-1102 (1999).
65. C. Waelbroeck *et al.*, *Nature* **412**, 724-727 (2001).
66. D. J. R. Thornalley, I. N. McCave, H. Elderfield, *Journal of Quaternary Science* **26**, 190-198 (2011).
67. V. L. Peck *et al.*, *Earth and Planetary Science Letters* **243**, 476-488 (2006).
68. W. E. N. Austin, E. Bard, J. B. Hunt, D. Kroon, J. D. Peacock, *Radiocarbon* **37**, 53-63 (1995).
69. J. Zhang, M. Steele, *Journal of Geophysical Research-Oceans* **112**, 10.1029/2006jc003732 (2007).
70. J. D. Guthrie, J. H. Morison, I. Fer, *Journal of Geophysical Research: Oceans*, DOI 10.1002/jgrc.20294 (2013).

Acknowledgments.

We thank Lloyd Keigwin, Tom Marchitto, Jerry McManus and Delia Oppo for discussions and comments on the manuscript. DJRT is grateful to Trond Dokken for suggesting looking to the Arctic Mediterranean for the source of poorly ventilated water reconstructed south of Iceland. Funding was provided by a WHOI OCCI scholarship and OCCI grant 27071264 (DJRT); WHOI OCCI and NSF grants OIA-1124880 and OCE-1357121 (GG); the WHOI J. Lamar Worzel Assistant Scientist Fund, the Penzance Endowed Fund in Support of Assistant Scientists and NSF ANT-1246387 (WG); EU FP7 Marie Curie grant No. 298513 (MZ), grant DP140101393 (JY); and NERC grant NE/J008133/1 (SB). Research was planned and performed by DJRT; except sample material, faunal counts and MD992276 Nps $\delta^{18}O$ were provided by HAB; WG, MZ and SMB conducted clumped isotope measurements; and GG conducted the idealized 1-D modelling. The manuscript was written by DJRT, with comments and contributions from all authors. Data used in this study can be found within the SOM.

Fig. 1. (**A**) Map showing core sites: red star, PS1243, 2.7 km; blue star, RAPiD cores (1P, 4P, 5P), S. Iceland Rise. Grey arrow, modern Nordic Seas overflow, orange arrows, surface inflow of North Atlantic Current (NAC). Approximate extent of ice sheets during the LGM are also indicated by light blue dashed line (after (*26*)) and dark blue dashed line indicates the extent of the Arctic Ocean (AO) at the shelf edge during the LGM when sea level was lowered. (**B**)

Schematic cross section through the AM as indicated by black line in (A); after (*1*). Deep and intermediate convection occurs in the Greenland and Norwegian Sea, while the deep Canadian basin may be ventilated by sinking of small volumes of brine enhanced shelf water (*1, 30*). Dashed lines are schematic isopycnals. Deep water exchange between the AM and the North Atlantic is restricted by the Greenland-Scotland Ridge, with a depth of ~400-800m.

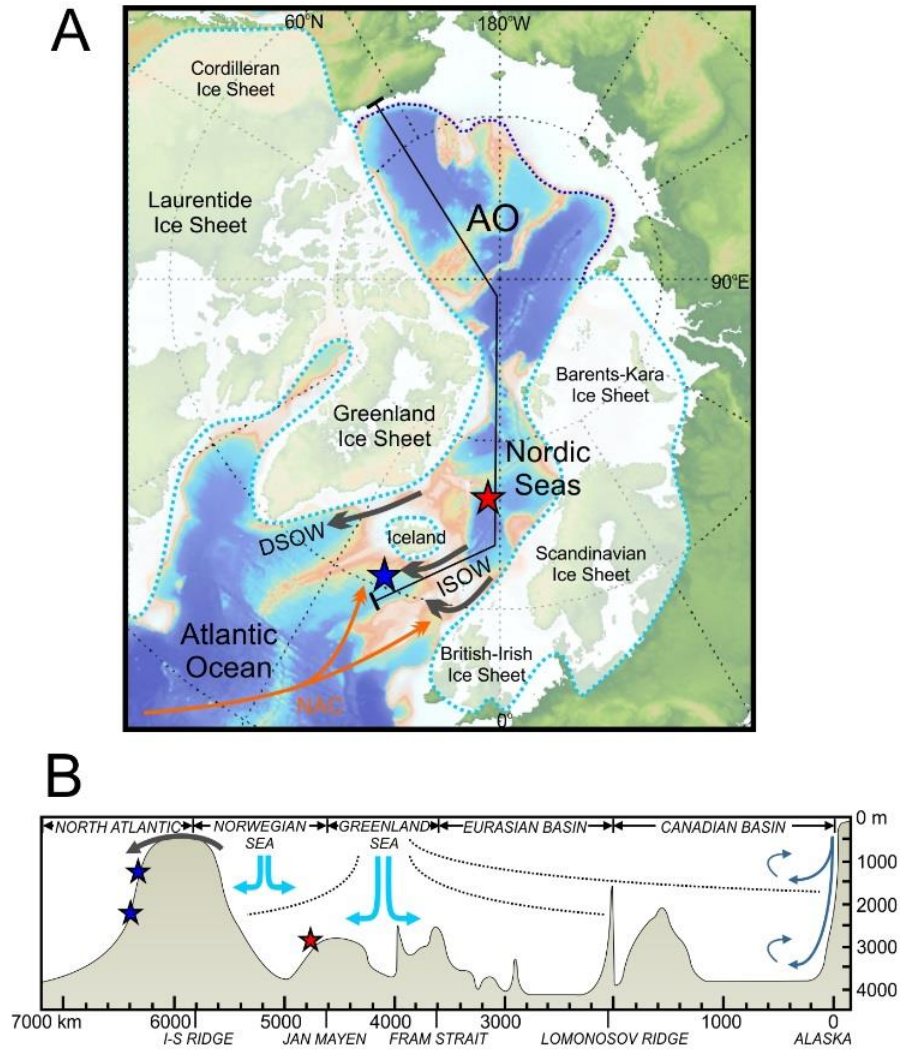

Fig. 2. (**A**) $\Delta^{14}C$ from the deep Norwegian Sea core PS1243 (black squares, benthics; grey circles, planktics), and S. Iceland Rise (1.2-2.3 km depth) (benthics, dashed grey) (*12*) with IntCal09 (*40*). Projection age extrapolation for samples at 23 ka shown by black dashed line (**B**) *C. wuellerstorfi* $\delta^{13}C$ from PS1243 (*19*). (**C**) Age model for PS1243; white circles, tie-points based on planktic ^{14}C using the modern reservoir age of 400 years; black circles, stratigraphic tie-points based on correlation of *N. pachyderma* (s) $\delta^{18}O$ shown in (**D**) by black arrows, the occurrence of the Vedde Ash and an abrupt decrease in % *N. pachyderma* (s) (not shown) at the onset of the Holocene. (**D**) Correlation of *N. pachyderma* (s) $\delta^{18}O$ between PS1243 (black) (*19*) and Norwegian Sea cores ENAM93-21 (solid grey) and MD95-2010 (dashed grey), that have been placed on the GICC05 age scale of NGRIP (**E**) via their magnetic susceptibility (*5, 41*).

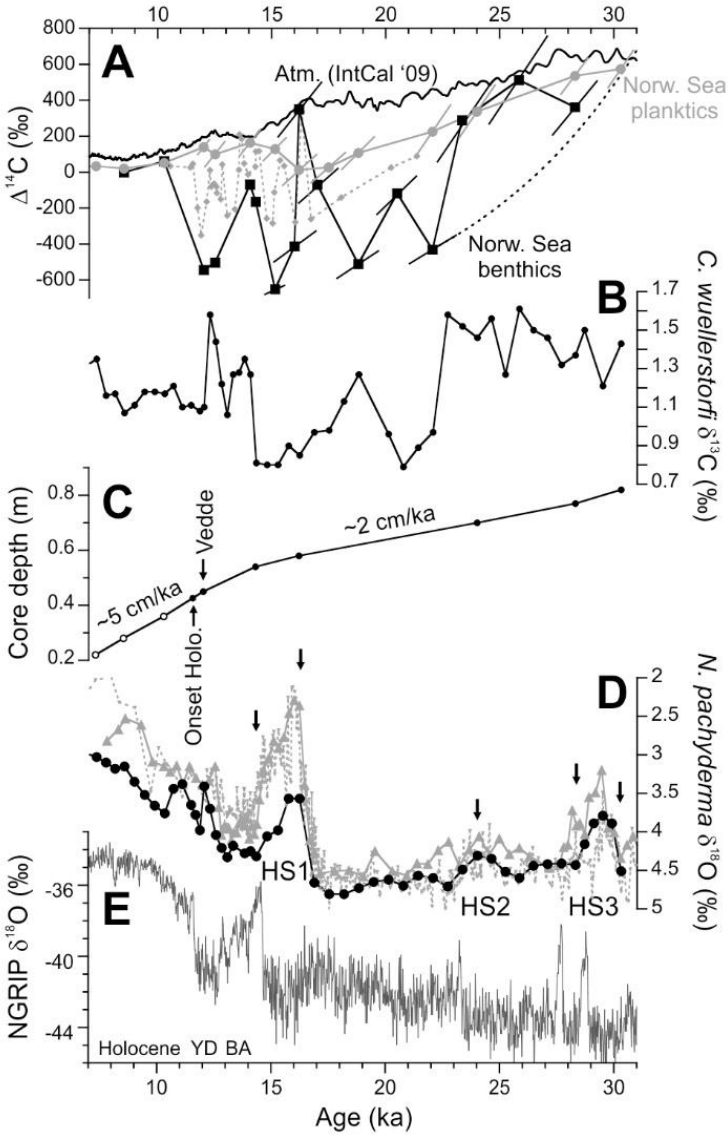

Fig. 3. Cross plot of *Cibicidoides* $\delta^{13}C$ and benthic-atmosphere ^{14}C ventilation age (log. scale), modified from (*12*). Black circles are new data from the deep Norwegian Sea; grey data are from the RAPiD cores on the South Iceland Rise.

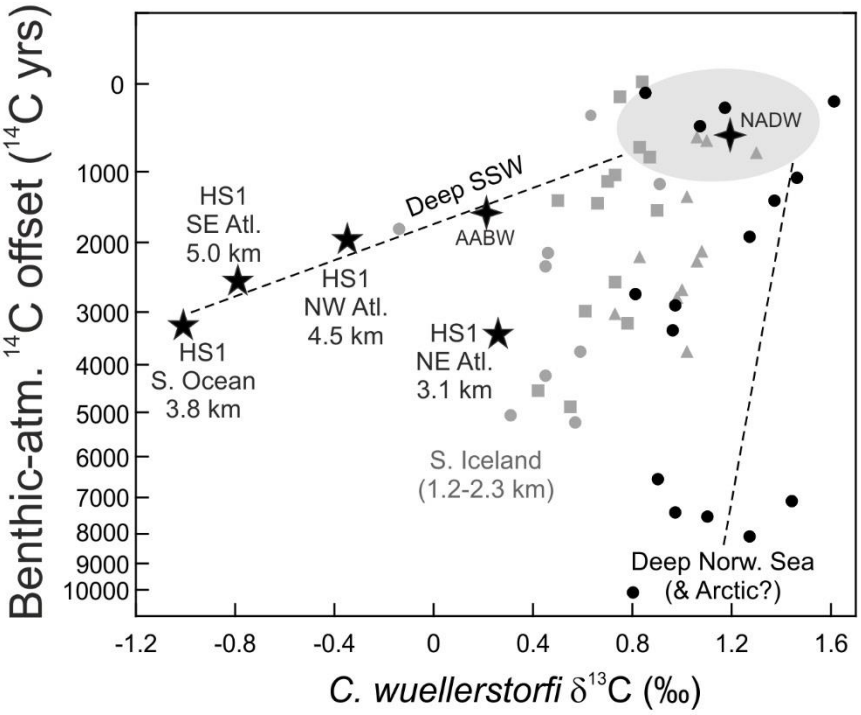

Fig. 4. Cartoon of hypothesised changes in circulation and ventilation of the Arctic, Nordic Seas and Northeast Atlantic (north to the right). Colour shading indicates ^{14}C ventilation. Pale blue layer indicates varying extent of surface freshwater and sea-ice/ice bergs (white rectangles). (**A**) Surface waters flow around the Nordic Seas and Arctic, losing buoyancy on route; ventilation of the intermediate and deep AM occurs mainly by convection in the Nordic Seas. (**B**) Reduction of deep convection and accumulation of poorly-ventilated dense water in the deep AM, resulting in a sharp radiocarbon front (see SOM). (**C**) Entrainment and/or overflow of aged AM water into the North Atlantic during HS1.

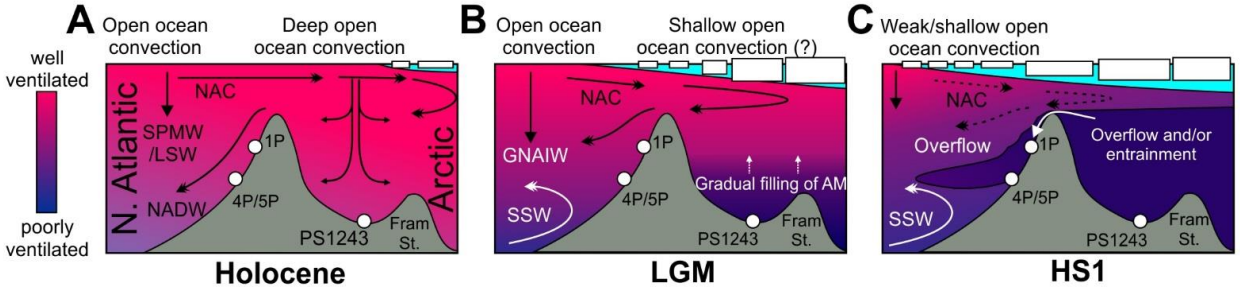

Fig. 5. (**A**) Benthic $\delta^{18}O$ from PS1243 (*19*), *Pyrgo depressa* (grey squares; vital effect -0.9ă), *C. wuellerstorfi* (grey circles) and *Oridosarlis umbonatus* (black diamonds; vital effect -0.28ă) with global sea level scaled to a 1ă whole ocean $\delta^{18}O$ change. The low $\delta^{18}O$ values of *C. wuellerstorfi* are discussed in the SOM. (**B**) Deep Norwegian Sea glacial-to-Holocene temperature change, with ±1σ errors, based on new clumped isotope data (Δ_{47}, horizontal grey line with error shading) and published ostracod Mg/Ca (grey circles) in PS1243 (*35*), and new benthic foraminifera Mg/Ca (black diamonds) in MD99-2276 (same core site as PS1243 ï see SOM). (**C**) Sample mean Δ_{47} measurements from *P. depressa* (squares) and *C. wuellerstorfi* (traingles) in PS1243 with averages and ±2 standard error shading for Holocene, deglacial and glacial intervals. ócore-topô foraminifera Mg/Ca and Δ_{47} data points are from (*42*) and (*43*) respectively.

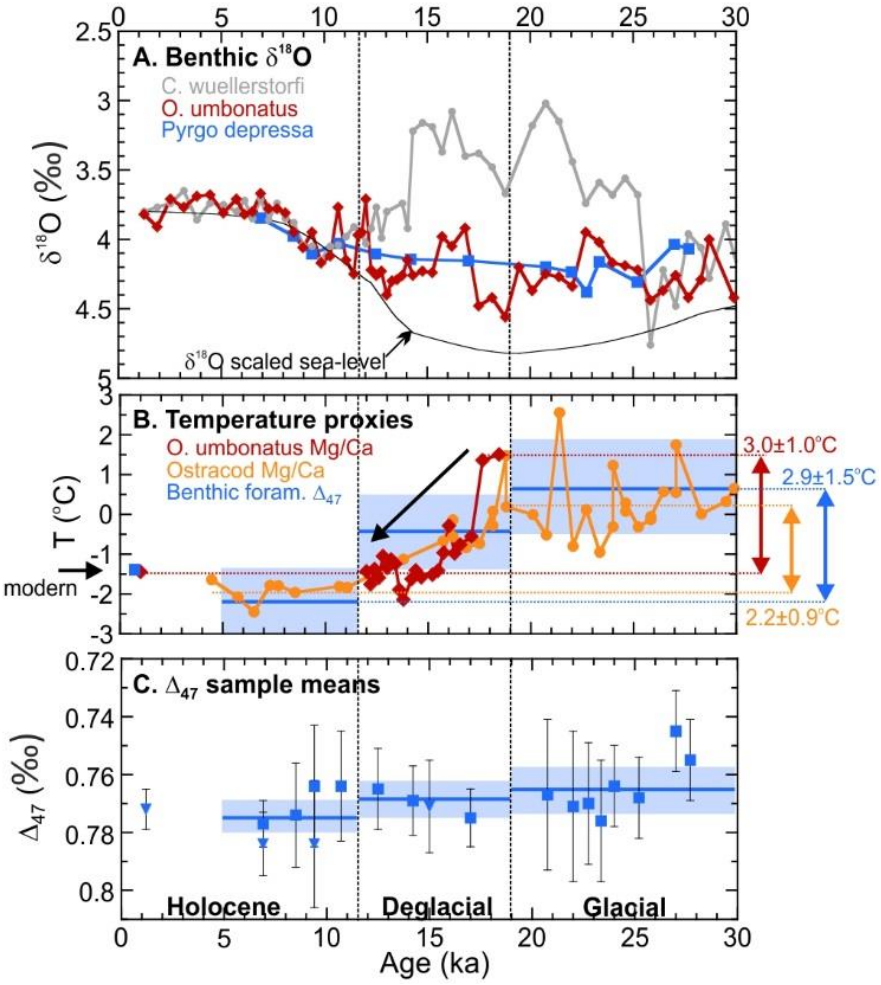

Table 1. Benthic ^{14}C data from PS1243. Intervals for benthic dates selected based on local abundance peaks where available (see SOM). For some samples a robust B-P age is not provided because there is no planktic ^{14}C date at the exact corresponding core depth.

	Depth (m)	Cal. Age (ka)	Species	^{14}C age (yrs)	Error (yrs)	B-P (yrs)	Error (yrs)	B-atm. (yrs)
Holocene	0.28	8.52	Cw	8290	35	170	100	570
ñ	0.28	8.52	Pyrgo	8090	75	-30	110	370
ñ	0.36	10.29	Cw	9530	40	-70	100	340
YD - Vedde	0.45	12.03	Cw	18000	100	7370	140	7760
YD	0.47	12.52	Pyrgo	17800	150	6400	160	7310
BA	0.53	14.05	Pyrgo/Cw	14250	65	1810	91	2030
ñ	0.54	14.30	Miliolids	15350	100	N/A		2930
HS1	0.56	15.15	Pyrgo	23200	250	9450	290	10400
ñ	0.575	16.00	Cw	19850	130	N/A		6710
	0.58	16.20	Pyrgo	13350	60	-2300	140	172
	0.595	17.00	Pyrgo/Cw	17100	95	N/A		3110
Late glacial	0.62	18.80	Miliolids	24000	290	6550	350	8370
ñ	0.645	20.50	Miliolids	20900	160	N/A		3530
ñ	0.67	22.05	Miliolids	26000	270	6210	340	7640
Early MIS 2	0.69	23.35	Pyrgo	20700	660	N/A		1220
ñ	0.73	25.84	Pyrgo	21800	220	N/A		270
ñ	0.77	28.30	Miliolids	25000	240	950	350	1520

Supplementary Materials for

A Warm and Poorly Ventilated Deep Arctic Mediterranean During the Last Glacial

D. Thornalley, H. Bauch, G. Gebbie, W. Guo, M. Ziegler, S. Bernasconi, S. Barker, L. Skinner, J. Yu.

Correspondence to: d.thornalley@cantab.net

This PDF file includes:

Materials and Methods

Core location and age model

Material was obtained from sediment core PS1243 (2711 m water depth, 69.37 N, 6.55 E), located within the central Norwegian Sea, presented in ref. (*19*). Today the deep Norwegian Sea is supplied by the products of deep convection in the Nordic Seas (mainly via deep convection in the Greenland Sea) and the outflow of Arctic Ocean Deep Water (AODW) via Fram Strait (*1, 28*). AODW forms through: (i) inflowing deep waters from the Norwegian Sea, (ii) the densification of Atlantic water through cooling and freezing and (iii) the formation of brine-enhanced shelf waters dense enough to descend from the shallow continental shelf into greater depth (*30*). Whereas the Nordic Seas and Eurasian Basin are relatively well ventilated, the deep (>2250 m) Canadian Basin, which is not ventilated by deep water formed in the Nordic Seas, has an isolation age of ~450 years (*44*). It is inferred either that the deep Canadian Basin underwent a vigorous convection event ~500 years ago and has since remained isolated (*37*), or it is instead subject to slow but relatively constant rates of deep water renewal (totaling ~0.1 Sv) by brine enhanced shelf water formation (~0.01 Sv) and subsequent entrainment during off-shelf transport (*30*).

The initial age model for PS1243 was based on planktic ^{14}C using the modern reservoir age of 400 years (*19*). Because previous work has demonstrated that large increases in reservoir age occur in this region during the deglaciation, especially HS1, we decided to use stratigraphic tie-points (Fig. 2), based on correlation of the low *N. pachyderma* (s) $\delta^{18}O$ events recorded throughout the Nordic Seas during H-stadials, between PS1243 and Norwegian Sea cores ENAM93-21 and MD95-2010, that have previously been placed on the ice core age scales via their magnetic susceptibility (*5, 41*), an approach also demonstrated in ref. (*45*). The smaller amplitude of the change during late HS1 at PS1243 reflects its greater distance from the collapsing Barents Sea ice-shelf, thought to be the major cause of the low $\delta^{18}O$ (*3*). This age model results in planktonic reservoir ages during HS1 of up to ~2400 years, in agreement with previous work in this region (*17*). Implied sedimentation rates are relatively constant. It is important to note that our main conclusions are not altered depending on whether a planktonic ^{14}C or stratigraphic based age model is used because B-P ^{14}C ages are not dependant on assigned calendar age, and adjustments to the benthic-atmosphere ventilation ages are modest compared to the magnitude of the signal (ventilation ages of up to 10,000 years are reduced at most by ~2000 years during HS1, and between 0 and 800 years for other intervals).

Alignment of MD99-2276 with PS1243

Because *Oridorsalis umbonatus* had already been used in PS1243 for stable isotope analyses, to obtain specimens for Mg/Ca-temperature analysis we used the neighbouring core from the same site, MD99-2276. This core was aligned with PS1243 via planktic and benthic stable isotopes and planktic ^{14}C ages, as shown in Fig. S1. Abundances below ~19 ka were too low to permit Mg/Ca analysis, while the core section above the Vedde Ash was disturbed during coring and so not suitable for analysis.

Temperature proxy data

***O. umbonatus* Mg/Ca from MD99-2276**

Mg/Ca data was obtained from *O. umbonatus* picked from MD99-2276 from the 250-355µm fraction, using 20-50 tests. Samples were cleaned at Cardiff University using the oxidative cleaning method of (*46*). Samples were dissolved in trace metal pure 0.065M HNO_3 and diluted with trace metal pure 0.5M HNO_3 to a final volume of 350 µl. Samples were analysed at Cardiff University on a Thermo Element XR ICP-MS against standards with matched calcium concentration to reduce matrix effects. Samples were screened for contaminant phases: Fe/Ca < 50 µmol/mol, Mn/Ca < 20 µmol/mol and Al/Ca < 25 µmol/mol, indicative of effective cleaning and negligible contaminate phases. Mg/Ca ratios were converted to paleo-temperatures using the published *O. umbonatus* calibration (*42*), after applying a 10% correction for the effects of the more corrosive cleaning technique employed in the calibration study (*46*):

$$Mg/Ca = 0.12 * T + 1.4 \text{ mmol/mol}$$

In Fig. 5, the ñcore-topò value plotted for our site at 2711 m in the Norwegian Sea, is the average core-top *O. umbonatus* Mg/Ca obtained from nearby Norwegian Sea cores KNR177-2 MC21 and MC45, 2640 m and 2799 m water depth from ref. (*42*).

Clumped isotopes analysis of benthic foraminifera in PS1243

To gain further support for the warmer glacial temperatures of the deep Norwegian Sea based on ostracod Mg/Ca and benthic foraminifera Mg/Ca, monospecific samples of *Pyrgo depressa* and a limited number of samples of *C. wuellerstorfi* from the >250 µm fraction were obtained from PS1243, and where enough material was available, crushed, split and analysed for carbonate clumped isotopes at two laboratories: ETH Zurich and Woods Hole Oceanographic Institution (WHOI).

WHOI measurements: Carbonate clumped isotope measurements at WHOI were performed on a Thermo Scientific MAT 253 mass spectrometer. CO_2 gases were generated from carbonate samples and standards, and purified using a custom-built, automated acid reaction and gas purification line. CO_2 gas standards, including ñheated gasesò (heated in quartz tubes in a muffle furnace at 1000ºC) and ñequilibrium gasesò (equilibrated with water in a glass flask at 40ºC), were also processed using the same purification line and analyzed to convert all the clumped isotope values into the absolute reference frame (*47*). This purification line at WHOI is very similar to the ones described by Passey et al. (*48*) and Henkes et al. (*49*), except the way how the ñequilibrium gasesò and ñheated gasesò were introduced to the system (see details below).

Foraminifera samples were measured over three analytical sessions between January and March of 2014 (31 aliquots over 01/13/2014-02/07/2014, 24 aliquots over 02/13/2014-03/03/2014, 2 aliquots over 03/05/2014-03/31/2014). During each measurement, 3-4mg of foraminifera tests were reacted *in vacuo*, for 10 min (session #1) or 20 min (session #2 and #3), in a common acid bath containing phosphoric acid (ρ=1.92g/ml) held at 90ºC. The CO_2 gases were then cryogenically purified with a -78ºC water trap (dry ice/ethanol slush) and passed through a custom-built 60 cm gas chromatography column containing Porapak^{TM} Q polymer (50-80 mesh) held at -20ºC. The flow rates of the He carrier gas were 25 ml/min (session #1) or 30 ml/min (session #2 and #3). Between runs this column was baked at 150ºC for about 90 min with a He flow of 10 ml/min. During analytical session #1, óequilibrium gasesô were introduced by directly freezing them in a liquid nitrogen trap after passing through a -78ºC water trap (dry ice/ethanol slush), while óheated gasesôwere introduced via the He carrier gas. During analytical session #2 and #3, óheated

gasesôwere also introduced by directly freezing them in a liquid nitrogen trap after passing through a -78ºC water trap.

Purified CO_2 gases were analysed at a bellow pressure corresponding to a signal of 12V on the Faraday cup measuring mass 44 CO_2. Each measurement sequence consists of six acquisitions, and each acquisition consists of 9 cycles of sample-reference comparison with 20 seconds of integration time. Two carbonate standards, NBS-19 and 102-GC-AZ01, were analysed regularly over all three sessions, yielding average values of 0.378±0.013ă (n=4), 0.394±0.006ă (n=8), 0.404±0.006ă (n=10) respectively for NBS19, and 0.710±0.004ă (n=19), 0.715±0.006ă (n=11), 0.712±0.003ă (n=11) respectively for 102-GC-AZ01. These values agree well with the average values from other clumped isotope laboratories for these carbonate standards, 0.392±0.017ă (1 standard deviation) and 0.713±0.012ă respectively (*47*). An acid digestion fractionation of 0.092ă was applied to derive the clumped isotope composition of all carbonate standards and samples reported here (*49*).

ETH measurements: Carbonate isotopologue measurements at the ETH in Zürich, Switzerland, were performed using a *Thermo Scientific Kiel IV* carbonate device (Thermo Fisher Scientific, Bremen, Germany) coupled to a *Thermo Scientific MAT 253* isotope ratio mass spectrometer as described by Schmid and Bernasconi (*50*) including an additional Porapak trap (*51*). The trap is inserted between the two cold fingers of the *Kiel* device and is filled for a length of about 2 cm with Porapak Type Q 50-80, glass wool, and silver-wool added at both ends of the trap to remove sulfur. During the run, the trap is cooled to -20°C. Between runs the trap is heated out for at least one hour at about 100°C.

The ETH approach involves repeated measurements of small (150-200 µg) subsamples, prepared individually in a *Thermo Scientific Kiel IV* carbonate device. Depending on the available amount of carbonate, between 8 and 48 aliquots were measured from the foraminifera samples. Before measurement, foraminifera were gently crushed between two glass plates. Sediment infill was removed and subsequently clean pieces of carbonate were hand-picked and used for the measurement.

The Pressure Base Line (PBL) on all Faraday cups was determined on a daily basis by peak scanning at 4-5 different *m/z* 44 intensities as described in Bernasconi et al. (*52*) and subsequently used for correction. The full correction scheme is described in detail by Meckler et al. (*53*). In order to correct for mass spectrometer-specific scale compression, PBL-corrected Δ_{47} values were transferred to the absolute reference frame (*47*) by means of an empirical transfer function (ETF). An acid fractionation correction of + 0.064 ă was applied to the Δ_{47ARF}, which results from a linear scaling of the observed offset between 25°C and 90°C acid temperature (*49*) to our reaction temperature of 70°C.

Measurements were continuously monitored and corrected by repeated measurements of four in-house carbonate standards, which strongly differ in bulk isotopic composition and ordering state. In each run at least two of the standards were measured. Offsets between measured and accepted values of the standards ($\Delta\Delta_{47}$) were averaged within a moving window encompassing 11 standards. Average offsets were then subtracted from sample and standard results. The residual standard offsets were also examined to determine if changes in scale compression had occurred.

Observed long-term standard errors of the means for (PBL-corrected) standard measurements with 10 acquisitions have an average value of 0.011 ă . An error of 0.004 ă (corresponding to a 1°C error at 25 °C; ref. (*54*)) could be achieved with roughly 50 aliquots. The total uncertainty

associated with the measurement of Δ_{47} considering all data processing steps is slightly higher, however this raises the final errors only slightly (by 0.001 ă on average). Repeated measurements of the international standard NBS-19 (N = 3) yielded a Δ_{47} value of 0.388 ± 0.005 ă (1 S.E.) in the absolute reference frame, within the range of values recently reported by 3 other laboratories (*47*).

Combined results:

Results of the combined clumped isotope analyses are provided in Table S3. No difference (at ±1 S.E.) is observed between *C. wuellerstorfi* and *P. depressa* data. To reduce the errors on estimated temperatures, samples were combined from three main intervals: Holocene (5-11.5 ka), deglacial (11.5-19 ka) and glacial (19-30 ka) (Fig. S2), which were selected based on the main trends observed in the benthic foraminifera Mg/Ca and ostracod Mg/Ca data (Fig. S2).

To combine and compare results from the two laboratories, 5 standards (NBS-19, ETH-1,2,3 and 4) were run multiple times (minimum of 3 analyses per standard) by both laboratories. An offset of 0.0145±0.003ă was observed between the laboratories, with heavier values recorded by WHOI. This inter-laboratory offset is similar in magnitude to that observed in an inter-laboratory comparison study (*47*). A -0.0145ă correction was subsequently applied to the WHOI data. This is consistent with the observation that without an inter-laboratory correction, WHOI Δ_{47} values for PS1243 samples were 0.013 and 0.015 ă heavier for the Holocene and glacial, respectively (p values < 0.05); applying the offset of 0.0145 obviously brings the two datasets into alignment (Table S4). It is important to note that, independently, results from both WHOI and ETH suggest warmer glacial temperatures. However by combining datasets, and thereby increases sample numbers, we are able to reduce the standard error of the estimated interval means.

Regardless of which specific calibration is used (e.g. using a theoretical calibration line (*49, 55, 56*) inorganic calcite (*57-59*) or one derived from biogenic carbonates (*43, 49, 58*)), the data suggest a ~2-3ºC warmer glacial deep Norwegian Sea, in agreement with the other temperature proxies. However the derived absolute paleo-temperatures can vary depending on which calibration is used, with a range of calibrations for various biogenic carbonates obtained from different laboratories e.g. (*49*). For example, the biogenic carbonate compilation calibration of ref. (*58*) results in temperatures that are several degrees too warm (~6-9ºC for Holocene, ~8-11ºC for glacial, depending on if we apply the 0.0145 ă correction to ETH or WHOI data), similar to observations made by (*43*). However, if we apply the calibration of ref. (*49*), derived from molluscs and brachiopods, using data on the ETH scale, we obtain temperatures of -2.2ºC for the Holocene and 0.7ºC for the glacial, in agreement with the other temperature proxy data. Although many of the samples used in ref. (*49*) are aragonitic, and our foraminifera are calcitic, the theoretically-predicted calcite calibration line ((*55*), recalculated in ref. (*49*)) also yields very similar temperatures. We have chosen to use the empirical biogenic calibration of ref. (*49*) to plot Δ_{47} temperature values in Fig. 5b because of its agreement with the two other temperature proxies. We stress that continued investigation and development of calibration lines and inter-laboratory comparison studies are clearly required. It is likely that future progress can be made by each laboratory developing and applying their own specific calibration. Yet the observation, from two independent laboratories, of 0.008-0.011ă lighter glacial Δ_{47} provides additional support for the benthic foraminifera and ostracod Mg/Ca paleotemperature data suggesting a 2-3ºC warmer glacial deep Norwegian Sea.

Supplementary Text

Benthic $\delta^{18}O$

One of the major issues regarding interpretation of benthic $\delta^{18}O$ in the deep Norwegian Sea is explaining why *C. wullerstorfi* $\delta^{18}O$ is ~1 ă lighter than other benthic species (*O. umbonatus* and *P. depressa*) during ~14-25 ka. This subject has been discussed at length in (*19*), where it has been suggested that because of their specific ecological preferences, and the fact that each sample interval represents a span of ~500 year, *C. wuellerstorfi* may be recording brief intervals where there is greater influence of low seawater $\delta^{18}O$, perhaps produced by episodes of brine-rejection and/or super-cooled $\delta^{18}O$-depleted ice-shelf water. Yet, some of these same samples also record very old ^{14}C-ventilation ages. Therefore either the source of low $\delta^{18}O$ water was also depleted in radiocarbon and/or we must envisage small volumes of highly $\delta^{18}O$-depleted water descending to the deep Norwegian Sea, entraining large volumes of poorly ^{14}C-ventilated water. For example, it is suggested that modern brine-enhanced shelf water plumes into the deep Canada Basin are diluted by a factor > ~5 (*30*). Alternatively, *C. wuellerstorfi* did not precipitate its calcite in equilibrium with seawater during this interval, although we are unaware of modern core-top data that might support this hypothesis. Alternatively, both *O. umbonatus* and *P. depressa* altered their vital effect by a similar amount during this interval, although given that they both show little variability across the glacial-deglacial period and track one another, this seems unlikely. Further investigation should be conducted into the change in $\delta^{18}O$ offset between *C. wuellerstorfi* and other benthics within the glacial and deglacial Norwegian Sea.

Another difficulty with interpreting benthic $\delta^{18}O$ changes within the deep AM is estimating the extent to which it was subject to the whole ocean glacial-interglacial shift in $\delta^{18}O$ of ~1 ă, given its poor ventilation and thus inferred isolation. Temperature proxy data suggests a 2-3ºC warming of the glacial deep AM. Therefore, it is plausible that the ~0.5 ă heavier glacial $\delta^{18}O$ was caused by the ~1 ă glacial whole ocean change combined with a warming of 2-3ºC, equivalent to ~0.5-0.75 ă, such that there was little-to-no local change in seawater $\delta^{18}O$. Yet we cannot discount the possibility that the deep AM was not subjected to the entire glacial-interglacial ~1 ă whole ocean shift and there was a significant change in local seawater $\delta^{18}O$ caused by changes in deep water formation processes. Regardless of these longer term shifts, we draw attention to the abrupt shift to ~2ºC colder temperature recorded by *O. umbonatus* Mg/Ca at ~17 ka (Fig. 5) that was accompanied by an opposing $\delta^{18}O$ decrease of ~0.3ă, implying a decrease in local seawater $\delta^{18}O$ of ~0.8ă, perhaps caused by mixing with overlying colder, low seawater $\delta^{18}O$ (hence likely fresh) waters, or alternatively, brine-rejection processes transferring a low seawater $\delta^{18}O$ surface signal to depth during this interval of HS1.

Feasibility test for old ventilation ages

To further investigate the impact of vertical diffusion and deep water formation rates on the age of waters in the AM, and the plausibility of obtaining ventilation ages of up to 10,000 years, we employ an idealized 1D-column advective-diffusive model for the AM. The results of various scenarios are outlined in Figures S4-S8. These demonstrate that, if modern estimates for vertical diffusivity are used, ventilation ages of 5-10,000 years are obtainable as long as rates of deep water renewal are kept below ~0.1 Sv. Furthermore, we are able to reconstruct the abrupt shift to old

ventilation ages as seen in core PS1243 through a simple idealized scenario described in Fig. S7 and S8.

Constraints on productivity to avoid anoxia in an aged Arctic Ocean

To calculate whether the aged Arctic Ocean of the past would have suffered from anoxia, we make a simple set of calculations from modern-day observations and our idealized model. Modern-day observations of dissolved oxygen in the central Arctic (*60*) show surface values near saturation (350 μmol/kg) and minimum oxygen layers at about 500 meters depth and in the abyss, with oxygen values of about 280 μmol/kg. Given that the abyss is typically ~500 years old (*44*), and that the oxygen utilization is the difference between the surface and abyssal values, then we have a rough estimate of the abyssal oxygen utilization rate: (70μmol/kg) / (500yr). We use the vertical particle flux profile diagnosed in a modern-day inverse model (*61*) [particle flux = $a*(Z/Z_{EZ})^{(-b)}$, in which $Z_{EZ,}$ the depth of the euphotic zone equals 133m; Z is water depth; and b=1.04] to derive the utilization rate within the water column. We can therefore obtain an estimate of the utilization rate at all depths by setting "a" to fit the observed abyssal utilization rate.

Using the physical state derived from the idealized model with bottom input of 0.08 Sv and vertical diffusivity of 10^{-5} m^2/s, we model the vertical profile of dissolved oxygen in the past ocean (Fig. S9), using the modelled water age and assigned oxygen utilization rate. First, we assume that the surface oxygen content is unchanged at 350 μmol/kg as the surface ocean cannot cool much further and thus cannot hold much more oxygen. Second, we assume that the oxygen utilization rate is proportional to the productivity, and we model cases where α, the fraction of productivity relative to the modern day, is varied between 1/100 to 1/5. We find that the past productivity in the Arctic must have been more than 10 times lower than the modern-day in order to avoid anoxic conditions at any depth (~20 times lower, for a bottom input of 0.04 Sv). However an important additional consideration is that this simple model scenario invokes a relatively poorly ventilated intermediate ocean (Fig. S5), yet reconstructions suggest the intermediate Nordic Seas, at least, remained well ventilated during the glacial (*17*), thus it is likely that lowering average productivity by a factor of ~5-10 times modern was sufficient to avoid anoxia in the deep AM.

In the central Arctic, glacial planktic foraminifera fluxes of <0.2 specimens cm^{-2} kyr^{-1} (compared to 2-10 specimens cm^{-2} kyr^{-1} for the Holocene (*32*)), suggest a >10-50 fold reduction in productivity. Counts from core PS1243, in the central Nordic Seas, reveal ~100-300 times lower flux of planktic and benthic foraminifera abundance during the last glacial, compared to the Holocene (this study and ref. (*19*)). The reduction in productivity during the last glacial was therefore likely sufficient to avoid anoxia.

We note that there are certain regions (e.g. the eastern Norwegian Sea and Fram Strait) where glacial productivity was not as suppressed (*32, 62*); yet these areas are not typical of the deep central Arctic Ocean or large parts of the Nordic Seas. Furthermore, these more productive regions are located within the Nordic Seas, where vigorous intermediate water formation and circulation during the glacial, e.g. (*17, 36*), would have prevented anoxia developing at intermediate depths (where remineralisation and oxygen utilization rates are highest). Our hypothesis of a poorly-ventilated glacial deep Arctic Mediterranean, with an overlying well-ventilated intermediate ocean, is therefore consistent with an oxygenated water column, based on our estimates of glacial surface productivity and oxygen utilization rates.

Faunal assemblage data precludes old ventilation ages being caused by bioturbation

A notable concern when using benthic foraminifera to reconstruct past seawater ventilation ages is that the foraminifera have been affected by bioturbation. We have clearly identified one interval in the core, at 0.50-0.51 m, which has been affected by a burrow that brought Holocene material downwards, resulting in an anomalous planktic (and benthic) assemblage and benthic and ówarmô planktic species radiocarbon ages that are impossibly young for the section of core below the Vedde ash (Fig. S10 and Table S1). This interval was previously interpreted to represent the Bølling-Allerød (BA) warm interval (*19*), but our new radiocarbon dates on the warm species demonstrate that it is a burrow containing Holocene material.

It is therefore necessary to pay considerable attention to whether it is possible that the extremely old inferred benthic ventilation ages elsewhere in the core may have been caused by upwards advection of material by bioturbation. Benthic faunal assemblage data are presented in Fig. S10, alongside the radiocarbon dates (and inferred ventilation ages). Although we cannot be fully confident that every single benthic ventilation age estimate has been unaffected by bioturbation, we are able to demonstrate that bioturbation cannot have caused the very old ventilation ages reconstructed at numerous depths within core PS1243, and instead they reflect the aging of the deep AM. Detailed examination of the benthic ventilation ages is provided below, and illustrated in Fig. S10.

***C. wuellerstorfi* ventilation ages.** Where abundance permitted, our preferred species for radiocarbon analyses was *C. wuellerstorfi* (Cw), because of its epifaunal habitat and widespread and demonstrated use in reconstructing past seawater chemistry. Ventilation ages consistent with the modern deep Norwegian Sea were obtained from Holocene samples. A well-defined abundance peak at 0.57-0.58 m yielded a benthic ventilation age of 6710 years. Because the abundance of Cw is an order of magnitude lower in the deeper section of the core, the Cw cannot have been bioturbated upwards (via advective or diffusive processes) from the older section of the core. Furthermore, the $\delta^{13}C$ at 0.57-0.58 m is 0.9ă , whereas Cw $\delta^{13}C$ from the older section of the core is ~1.5ă , inconsistent with upwards bioturbation of older material. We also obtained a Cw ventilation age of 7760 years at 0.45 m, chosen because it is at the base of the Vedde Ash, which provides a robust chronological marker. There is a large increase in abundance of Cw above this point, however this would tend to result in biasing of the ventilation age to younger ages, not older. As previously discussed, our other Cw date, at 0.51 m, comes from an interval affected by a burrow that has brought down Holocene material; the high abundance of Cw, high $\delta^{13}C$, high abundance of warm Holocene planktic fauna, and Holocene aged Cw and *G. bulloides* and *T. quinqueloba* (Table S1) are all consistent with this interpretation.

***Pyrgo* sp. ventilation ages.** *Pyrgo* species were utilised for benthic ventilation ages because individuals tend to be large and heavy, allowing enough calcite to be obtained for precise radiocarbon dating. Previous work from the Santa Barbara basin (SBB) has suggested *Pyrgo* sp. may not be suitable for benthic radiocarbon work, however this is a relatively unusual oceanic setting, and it is thought that the anomalously old ^{14}C ages, and $\delta^{13}C$ values of -4 to -8ă , were due to the shallow infaunal *Pygro* sp. calcifying in isotopically depleted (old) pore waters caused by the addition of tar (*63*). In contrast to the SBB results, our *Pyrgo* sp. $\Delta^{14}C$ data from the deep Norwegian do not display a consistent offset to more depleted values: our paired Cw and *Pyrgo* sp. data from the Holocene are in good agreement (ventilation ages of 570 years and 370 years),

and closely spaced samples of Cw and *Pyrgo* sp. from within the YD (0.45 m and 0.47 m) are also in good agreement (7760 years and 7310 years). We also note that the relatively high $\delta^{13}C$ of our glacial and deglacial *Pyrgo* sp. samples (0 to 0.8ă lower than Cw $\delta^{13}C$), suggests only a minor influence of isotopically depleted porewater. We are therefore confident that within the deep Norwegian Sea, *Pyrgo* sp. can be used to accurately reconstruct seawater ventilation ages.

Similar to the arguments made previously for Cw data, the 7310 years ventilation age obtained on *Pyrgo* sp. at 0.47 m cannot be caused by upwards bioturbation of older material because the deeper levels of the core have abundance of *Pyrgo* sp. that are an order of magnitude lower. If anything, this ventilation age estimate may be biased towards a younger age because of downwards bioturbation from the overlying Holocene where *Pyrgo* sp. are very abundant. We also dated a small abundance peak at 0.56-0.57 cm which yielded a ventilation age of 10400 years. Again, it is difficult to conceive that this resulted from upwards bioturbation of older material yet had no impact on the Nps ^{14}C age because this would require a strong increase in *Pyrgo* sp. abundance downcore which is not observed.

Mixed benthic ventilation ages. It was not always possible to obtain single genera benthic foraminifera ventilation ages, and therefore, to obtain a more complete deglacial record of ventilation changes, we had to use measurement made on mixed benthics. Two measurements were made on samples where we combined Cw and *Pyrgo* sp., on small abundance maxima. Neither measurements yielded exceptionally old benthic ventilation ages. It is possible that the Cw/*Pyrgo* date at 0.53 m was adversely affected by Holocene material from the burrow at 0.51 m, although the planktic faunal data do not indicate a substantial presence of Holocene (low %Nps) material. The relatively young ventilation age (2030 years) may instead record improved ventilation during the BA.

Where there was not sufficient material to perform Cw or *Pyrgo* sp. measurements, we analysed mixed *Miliolid* species (including *Pyrgo* sp.). Although these dates were not obtained from pronounced abundance maxima (notwithstanding our ^{14}C date taken at 0.77 m), and there is a slight increase in abundance of *Miliolid* species towards 1.0 m core depth, it seems unlikely that the old ventilation ages at 0.62 m (8370 years) and 0.67 m (7640 years) are caused by burrows bringing older material upwards, because the Nps ^{14}C dates are not anomalously old ï given there are no strong abundance gradients in Nps or *Miliolid* sp. between 0.62-0.67 m and ~0.8-1.0 m, it is unlikely that the *Miliolids* were bioturbated upwards but not the Nps. Furthermore, because we have identified several other intervals where we are confident about the fidelity of the $\Delta^{14}C$ reconstruction, it seems much more likely that the old ventilation ages measured using *Miliolid* sp. also reflect poor ventilation of the deep Norwegian Sea.

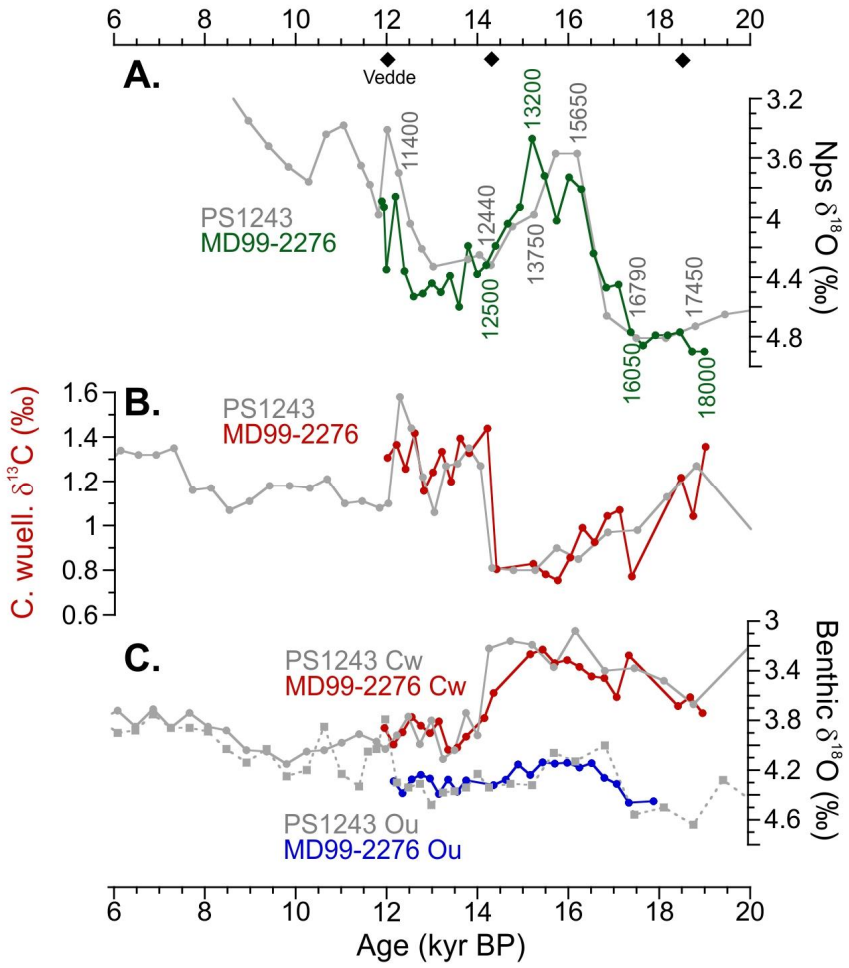

Fig. S1.

(**A**) MD99-2276 was tied to the PS1243 age model through correlation of Nps $\delta^{18}O$ (black diamonds, tie-points); radiocarbon dates on Nps confirm the age model. (**B**) *C. wuellerstorfi* $\delta^{13}C$ in PS1243 and MD99-2276. (**C**) *C. wuellerstorfi* and *O. umbonatus* $\delta^{18}O$ in PS1243 and MD99-2276; a vital effect offset of -0.28ă has been applied to the *O. umbonatus* $\delta^{18}O$.

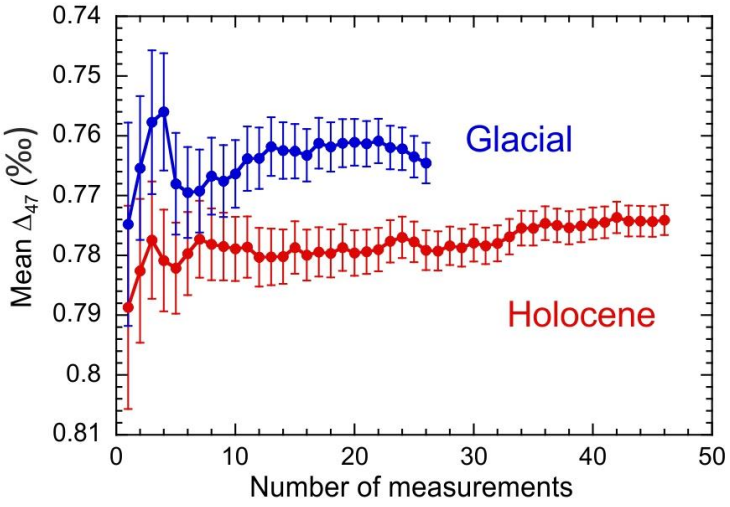

Fig. S2.

The standard error on the mean Δ_{47} value of benthic foraminifera samples from a given time interval is reduced through multiple measurements. Error bars are ±1 standard error.

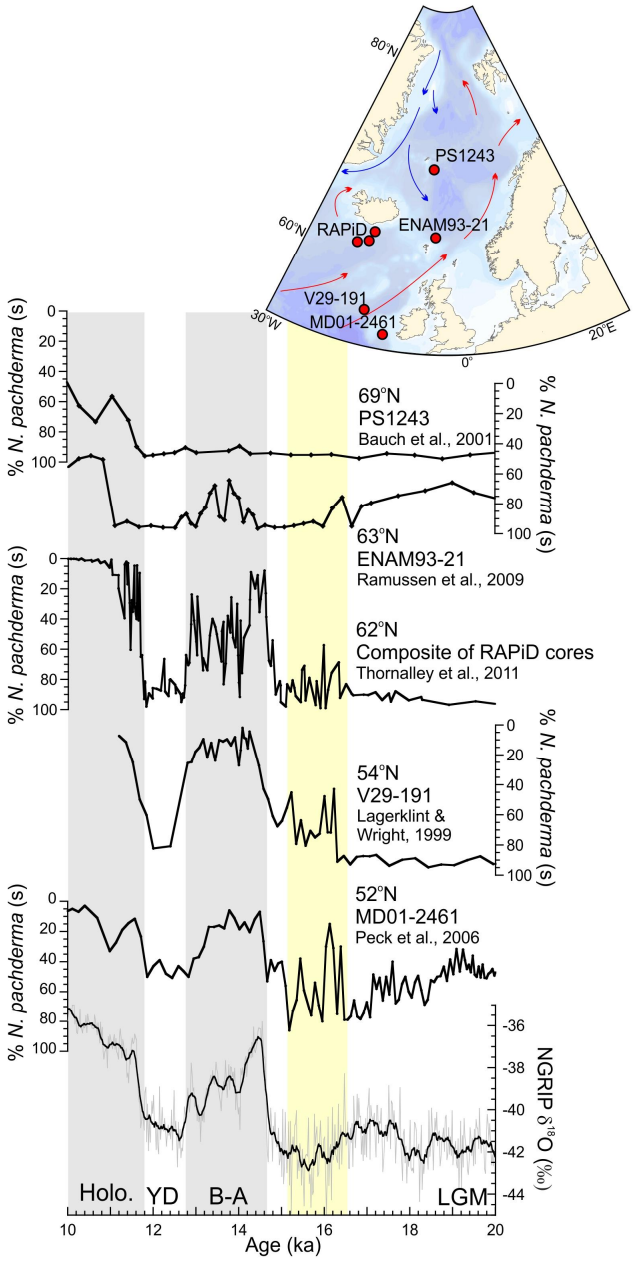

Fig. S3.

High resolution planktic faunal data from the subpolar Northeast Atlantic and Norwegian Sea. An ǿarlyô warming event, of weaker magnitude in northerly sites, is recorded at ~16 ka in the Northeast Atlantic records, coinciding with the convection event recorded in the deep Norwegian Sea (2.7 km) and on the South Iceland Rise (2.3 km). This faunal event is not clearly identified within the Norwegian Sea cores, suggesting limited penetration/extent of warmer (sub)surface water within the Norwegian Sea. Original cited age models are used, except for PS1243, which uses the age model of this current study, and V29-191, which uses the original planktic ^{14}C dates in (*64*), but a 1500 year surface reservoir age correction during HS1 and 700 year for the YD (rather than 400 year), based on the results of several previous studies in this region e.g. (*65-68*).

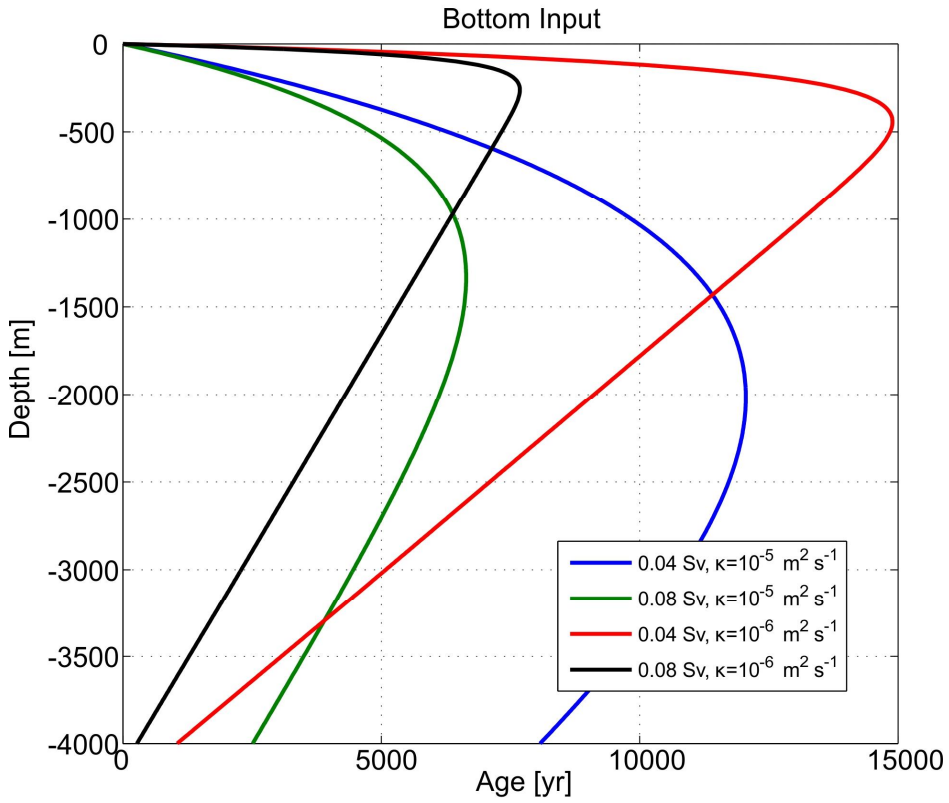

Fig. S4.

Age of waters in an idealized 1D-column Arctic model where young waters (age = 0 years) enter the water column at 4000 meters depth at a rate of 0.04 or 0.08 Sv, with a commensurate upwelling at all depths balanced by a vertical diffusivity of 10^{-5} or 10^{-6} m^2/s, with the surface set to an age of 0 years. In the low diffusivity (10^{-6} m^2/s) regime, the age profile linearly increases from the bottom at the rate of aging consistent with upwelling. In the higher diffusivity regime (10^{-5} m^2/s), diffusive processes counteract the upwelling, and water ages are greater at depth. Under plausible bottom water formation rates of 0.04 Sv, waters age by 10,000 years or more, with the vertical structure depending upon the vertical diffusivity, which for the modern central Arctic is suggested to be O(10^{-6} m^2/s) (*69, 70*).

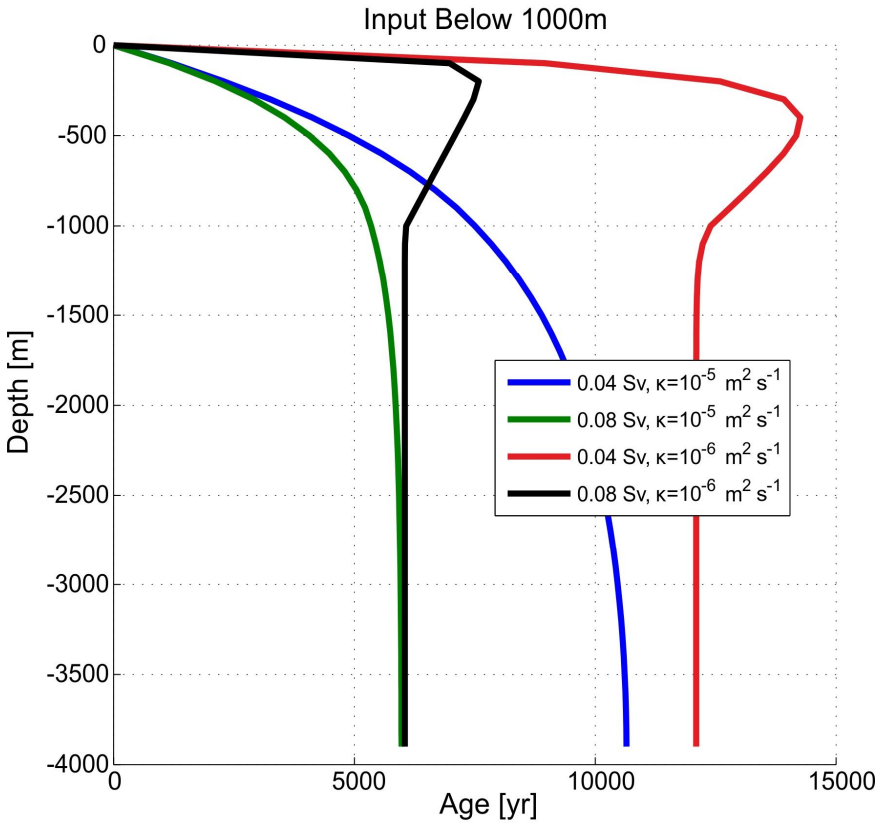

Fig. S5.

Similar to Fig. S4, but waters enter the column in equal proportions below 1000m depth. Waters age more than 10,000 years at the bottom in all cases where vertical diffusivity is between 10^{-5} and 10^{-6} m^2/s and the total input of young water is 0.04 Sv; younger ages are obtained for an input of 0.08 Sv, but still in excess of 5,000 years. The primary balance in the deep column is between the lateral addition of young waters and in-situ aging.

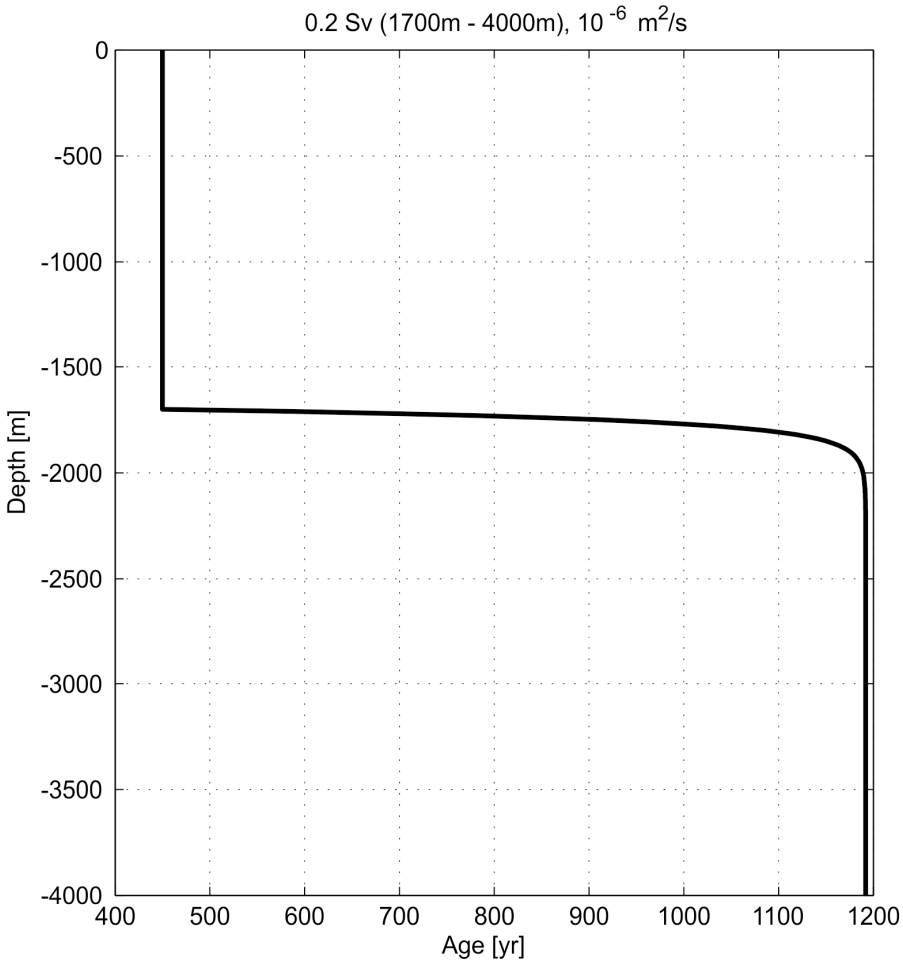

Fig. S6.

A modern analogue of the idealized 1D-column model of the Canadian Basin. In this check of the validity of the idealized model, waters above the halocline at 1700 meters depth are kept fixed at an age of 450 years, 0.2 Sv of 450-year-old water is introduced evenly from 1700m to 4000m depth, and the vertical diffusivity is the modern-day inferred value of 10^{-6} m^2/s. The layer interface at 1700m isolates a deep layer of Arctic water with an age of nearly 1200 years, reflecting an additional 750 years of aging that is roughly consistent with modern-day radiocarbon observations (*30, 44*).

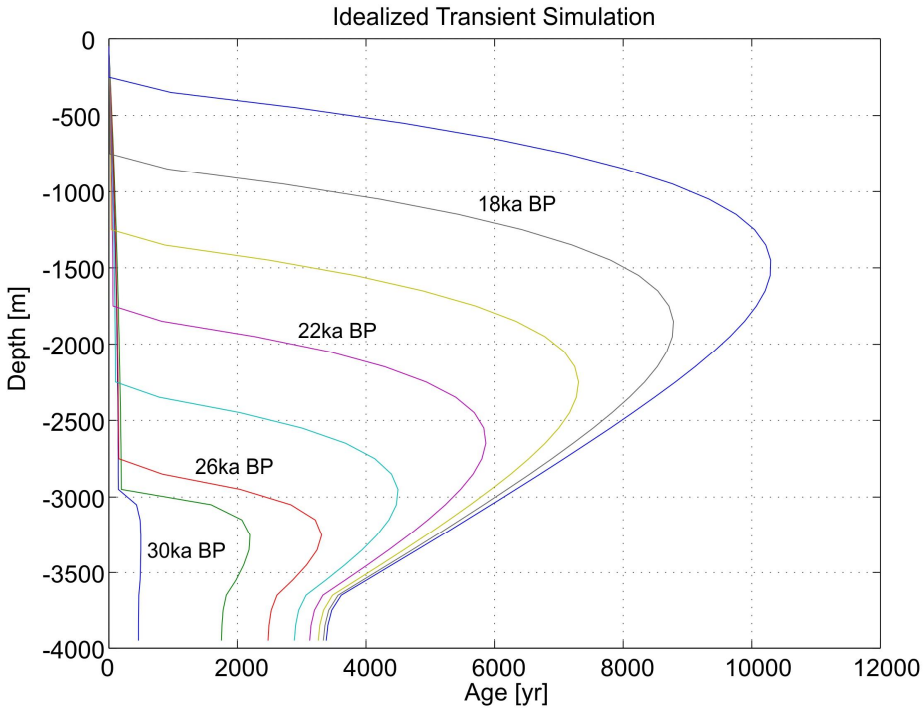

Fig. S7.

Progression of the age profile of a transient simulation where 0.04 Sv of (dense) bottom water fills, below 3500 m water depth, an initially well-ventilated AM water column (surface set to 0 years). A high diffusivity layer (10^{-3} m^2/s; simulating well mixed waters formed by convection) recedes from 3000 m depth to the surface at the rate of inflow of the bottom waters. The bottom water layer has a vertical diffusivity of 10^{-6} m^2/s.

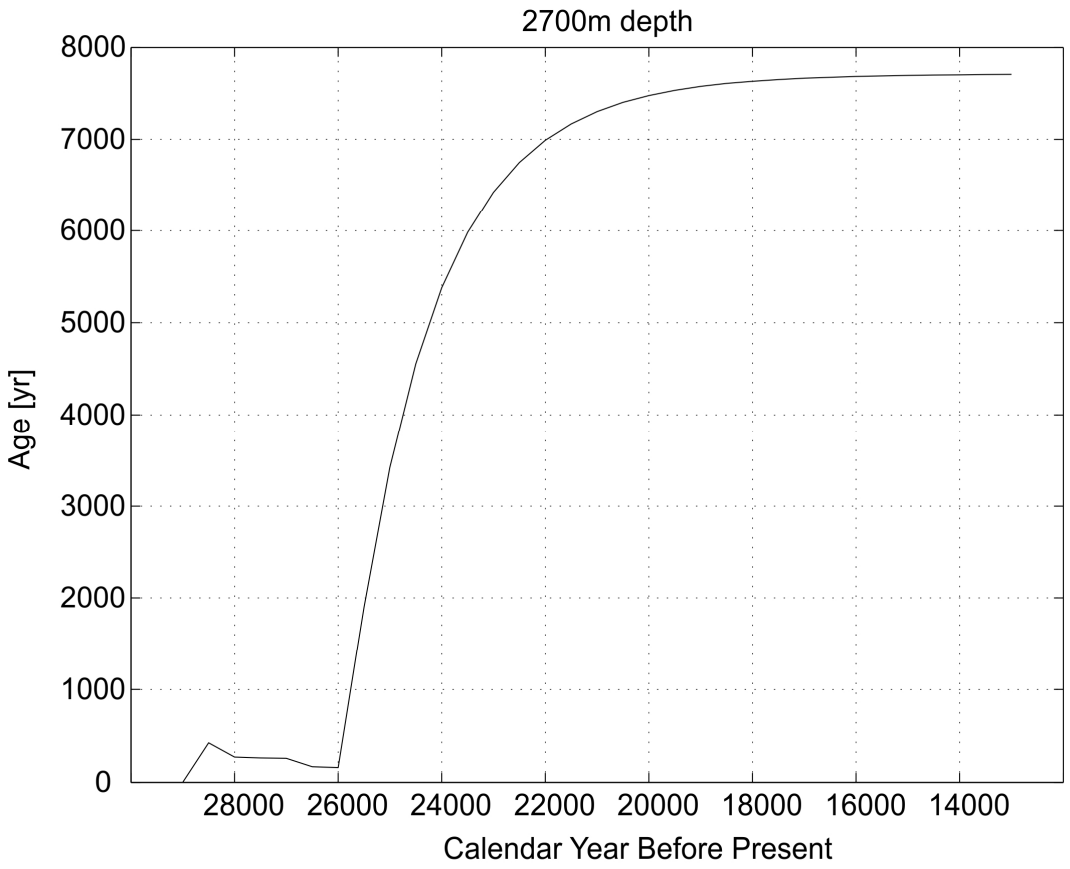

Fig. S8.

Time series of the aging of waters at 2700 meters depth from the transient simulation of Fig. S7. When young waters fill the basin past 2700 meters depth, a front with rapidly increasing age passes the depth level as well. Waters age by ~5000 years in a 2000 year interval, indicating that processes beyond in-situ aging are operating.

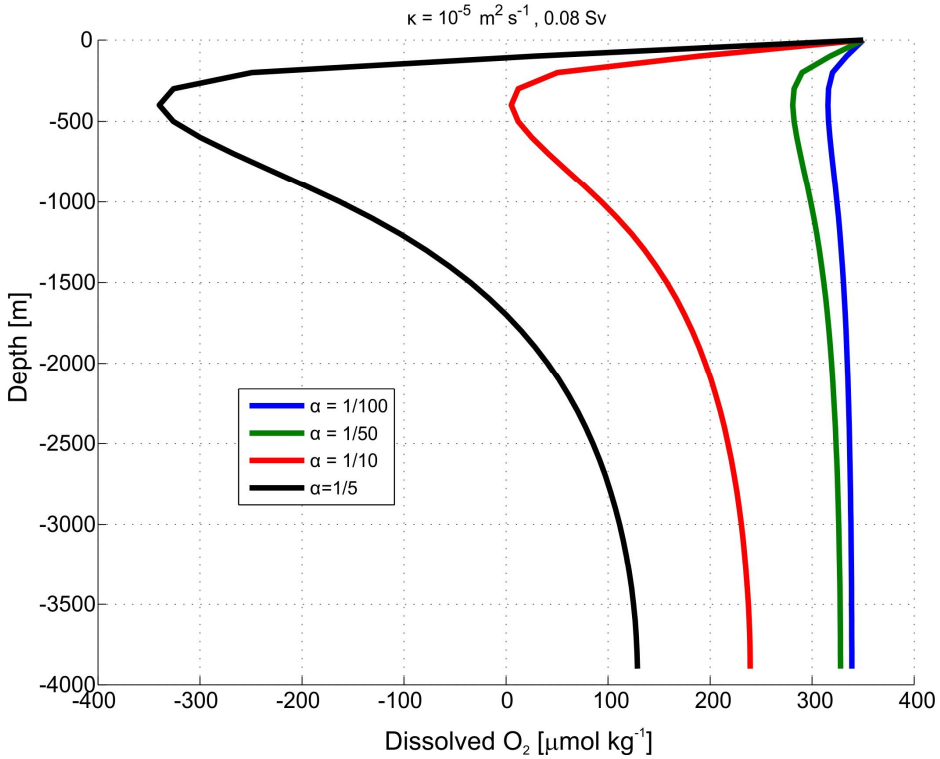

Fig. S9.

Dissolved oxygen concentration for an idealized 1D model of the Arctic with a bottom water input of 0.08 Sv and vertical diffusivity 10^{-5} m^2/s (see Fig. S4). Anoxic conditions are avoided as long as glacial Arctic surface productivity was 5-10 times lower than modern. It is also possible that there was a strong subsurface inflow and circulation of intermediate water (Atlantic Water) within the upper Arctic Ocean that would have helped ventilate intermediate depths (where remineralisation and oxygen utilization rates are highest) and thus prevent anoxia.

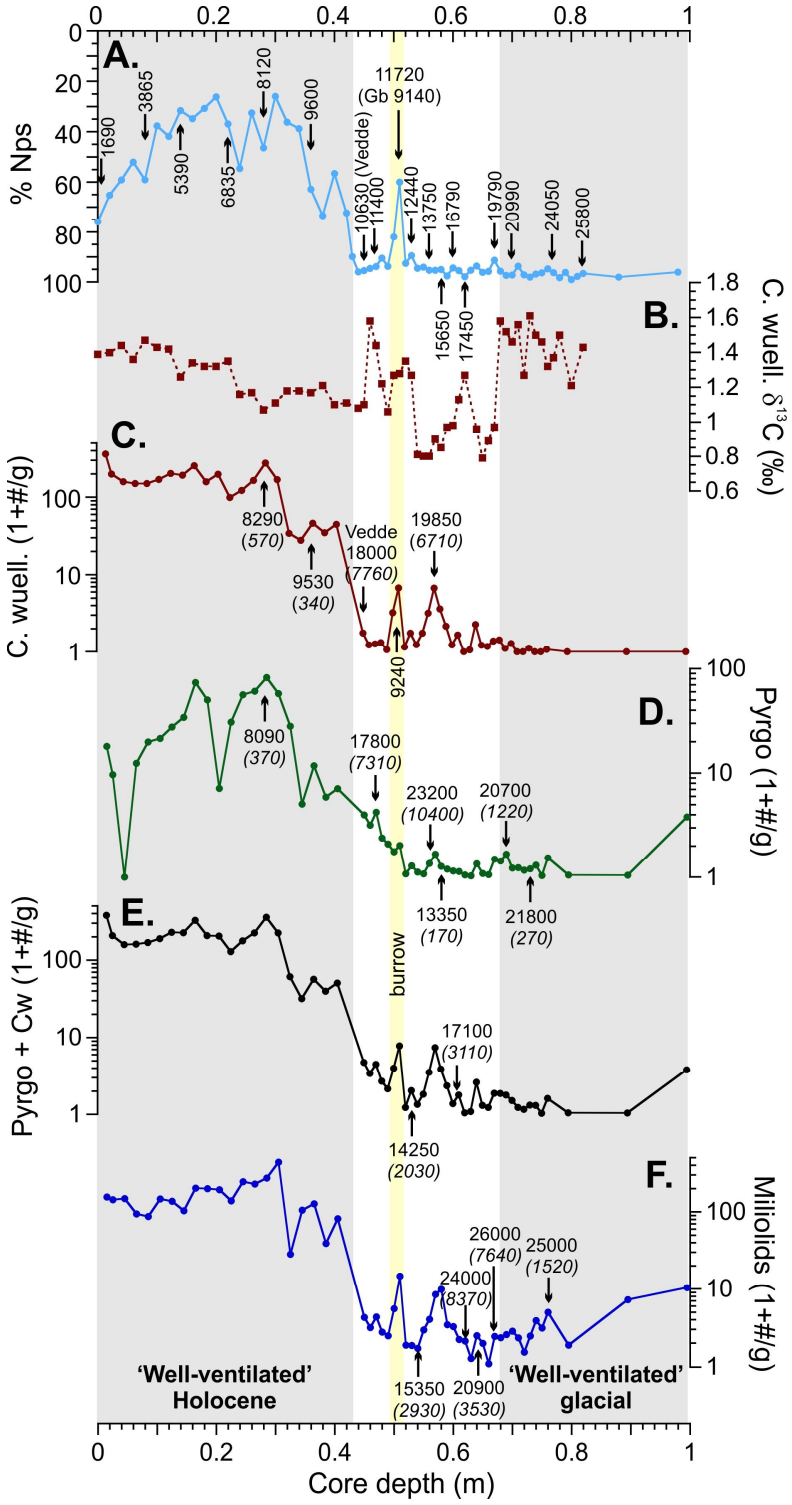

Fig. S10.

Faunal abundance data and radiocarbon ages (not calibrated or reservoir corrected) from PS1243. (**A**) % Nps, radiocarbon ages on Nps (and one *G. bulloides* date). (**B**) *C. wuellerstorfi* δ^{13}C. (**C-F**) Benthic faunal assemblage data and radiocarbon ages; benthic-atmosphere ventilation ages in parentheses.

Table S1 ï Benthic and planktic ^{14}C AMS measurements for core PS1243

	Depth (m)	Age (ka)	Species	Weight (mg)	^{14}C age (yrs)	Error (yrs)	$\delta^{13}C$ (ă)	Age-corrected $\Delta^{14}C$ (ă)	Cib. $\delta^{13}C$ (ă)	Offset from atm. IntCal09 (^{14}C yrs)
Benthics										
OS-95863	0.28	8.52	Cw	7.8	8290	35	1.16	-1	1.07	570
OS-105126	0.28	8.52	Pyrgo	6.1	8090	75	-0.4	24	1.07	370
OS-95864	0.36	10.29	Cw	8.5	9530	40	1.18	61	1.17	340
OS-95865	0.45	12.02	Cw	5.1	18000	100	0.96	-544	1.10	7760
OS-96587	0.47	12.52	Pyrgo	4.5	17800	150	1.21	-503	1.44	7310
**OS-95866*	*0.51*	*13.50*	*Cw*	*8.1*	*9240*	*40*	*1.24*	*N/A*	*1.28*	*N/A*
OS-95867	0.53	14.05	Cw/Pyrgo	3.1	14250	65	0.76	-69	1.27	2030
OS-96596	0.54	14.30	Miliolids	1.5	15350	100	0.39	-165	0.81	2930
OS-96588	0.56	15.15	Pyrgo	4.0	23200	250	0.77	-651	0.80	10400
OS-95868	0.57-0.58	16.00	Cw	5.4	19850	130	0.80	-413	0.90	6710
OS-95869	0.58	16.20	Pyrgo	6.9	13350	60	0.87	350	0.85	170
OS-95870	0.59-0.61	17.00	Cw/Pyrgo	4.0	17100	95	0.63	-70	0.97	3110
OS-96589	0.62	18.80	Miliolids	2.8	24000	290	0.83	-511	1.27	8370
OS-95871	0.64-0.65	20.50	Miliolids	4.5	20900	160	0.79	-118	0.96	3530
OS-95872	0.67	22.05	Miliolids	5.1	26000	270	0.86	-431	0.97	7640
OS-95873	0.69	23.35	Pyrgo	5.7	20700	660	0.84	289	1.46	1220
OS-96595	0.73	25.84	Pyrgo	2.3	21800	220	0.78	512	1.61	270
OS-95874	0.77	28.30	Miliolids	4.3	25000	240	0.60	362	1.37	1520
Planktics										
(a)	0	1.25	Nps		1690					(b)
(a)	0.08	3.82	Nps		3865					(b)
(a)	0.14	5.74	Nps		5390					(b)
(a)	0.22	7.30	Nps		6835					(b)
(a)	0.28	8.52	Nps		8120					(b)
(a)	0.36	10.29	Nps		9600					(b)
(a)	0.45	12.02	Nps		10630					390
OS-96590	0.47	12.52	Nps	8.4	11400	65	0.60	99		910
**OS-107184*	*0.50*	*13.30*	*Tq*	*4.6*	*8090*	*30*	*-1.49*	*N/A*		*N/A*
**OS-96591*	*0.51*	*13.50*	*Gb*	*4.0*	*9140*	*50*	*-0.09*	*N/A*		*N/A*
**KIA 42610*	*0.51*	*13.50*	*Nps*	*-*	*11720*	*55*	*-*	*N/A*		*N/A*
(a)	0.53	14.05	Nps		12440					220
OS-96592	0.56	15.15	Nps	8.2	13750	85	0.21	128		950
OS-96593	0.58	16.20	Nps	9.0	15650	130	0.14	13		2470
(a)	0.60	17.50	Nps		16790					2450
OS-96594	0.62	18.80	Nps	9.0	17450	120	0.17	107		1820
(a)	0.67	22.05	Nps		19790					1430
(a)	0.7	24.00	Nps		20990					840
(a)	0.77	28.30	Nps		24050					570
(a)	0.82	30.30	Nps		25800					380

(a) From ref. (*19*). (b) Assumed 400 yr (*19*)

*2 cm interval in the core likely affected by a burrow that has brought down early Holocene material, which is typified by high *C. wuellerstorfi* abundance and warm planktic foraminiferal assemblage (i.e. *G. bulloides* and *T. quinqueloba*), resulting in an anomalous abundance peak of

warm planktic species and *C. wuellerstorfi* (*19*). Because of the relatively low glacial abundance of *C. wuellerstorfi*, *G. bulloides* and *T. quinqueloba*, picking of these species will have been heavily biased towards selecting the Holocene material. In contrast, the high glacial abundance of *N. pachyderma* (sinistral) (Nps) (and lower abundance in the Holocene material) means the Nps date is less affected by the burrowed material, however we have not used this date in our final results.

Table S2 ï Planktic ^{14}C AMS measurements for core MD99-2276

	Depth (m)	Age (ka)	Species	Weight (mg)	^{14}C age (yrs)	Error (yrs)	$\delta^{13}C$ (ă)	Offset from atm. IntCalõ09 (^{14}C yrs)
OS-105124	1.07	14.2	Nps	9.3	12500	50	0.35	139
OS-105123	1.11	15.2	Nps	10.8	13200	55	0.20	300
OS-105122	1.19	17.1	Nps	7.9	16050	65	0.02	1781
OS-105121	1.25	19.0	Nps	8.7	18000	75	0.05	2017

Table S3. Clumped isotope data. Coretop sample is from ref. (*43*); $\delta^{18}O^*$ includes a vital effect of -0.9ă for *P. depressa*; $^*\Delta_{47}$ includes an offset of -0.0145ă for data from Caltech and WHOI labs.

	Species	Depth (m)	Lab.	Age (ka)	Runs #	$\delta^{13}C$ ă	$\delta^{18}O$ ă	$\delta^{18}O^*$ ă	Δ_{47} ă	$^*\Delta_{47}$ ă	SE ă
Coretop	C. wuell.	0 -0.01	Caltech	1.2	N/A	1.35	3.86	3.86	0.786	0.772	0.007
Holocene	P. depressa	0.20-0.21	WHOI	6.9	N/A	-0.36	4.93	4.03	0.782	0.767	0.009
	P. depressa	0.20-0.21	WHOI	6.9	N/A	-0.48	4.85	3.95	0.777	0.763	0.016
	P. depressa	0.20-0.21	WHOI	6.9	N/A	-0.52	4.69	3.79	0.799	0.784	0.018
	P. depressa	0.20-0.21	WHOI	6.9	N/A	-0.52	4.94	4.04	0.796	0.781	0.013
	P. depressa	0.20-0.21	WHOI	6.9	N/A	-0.52	4.94	4.04	0.797	0.782	0.012
	P. depressa	0.20-0.21	WHOI	6.9	N/A	-0.48	4.93	4.03	0.790	0.776	0.013
	C. wuell.	0.20-0.21	WHOI	6.9	N/A	1.74	3.88	3.92	0.813	0.799	0.010
	C. wuell.	0.20-0.21	WHOI	6.9	N/A	1.43	3.94	3.92	0.794	0.780	0.015
	C. wuell.	0.20-0.21	WHOI	6.9	N/A	1.40	3.92	3.92	0.794	0.780	0.016
	P. depressa	0.28-0.29	WHOI	8.5	N/A	-0.42	5.06	4.16	0.812	0.797	0.013
	P. depressa	0.28-0.29	WHOI	8.5	N/A	-0.42	4.99	4.09	0.790	0.775	0.017
	P. depressa	0.28-0.29	WHOI	8.5	N/A	-0.41	5.02	4.12	0.786	0.772	0.007
	P. depressa	0.28-0.29	WHOI	8.5	N/A	-0.43	5.02	4.12	0.761	0.747	0.009
	C. wuell.	0.32-0.33	WHOI	9.4	N/A	1.61	4.22	4.25	0.802	0.788	0.015
	C. wuell.	0.32-0.33	WHOI	9.4	N/A	1.37	4.26	4.25	0.770	0.755	0.015
	C. wuell.	0.32-0.33	WHOI	9.4	N/A	1.29	4.27	4.25	0.807	0.792	0.016
	P. depressa	0.32-0.33	WHOI	9.4	N/A	-0.08	5.13	4.23	0.780	0.766	0.007
	P. depressa	0.32-0.33	WHOI	9.4	N/A	-0.39	5.06	4.16	0.756	0.741	0.004
	P. depressa	0.32-0.33	WHOI	9.4	N/A	-0.36	5.02	4.12	0.743	0.728	0.011
	P. depressa	0.32-0.33	WHOI	9.4	N/A	-0.38	5.15	4.25	0.790	0.776	0.017
	P. depressa	0.32-0.33	WHOI	9.4	N/A	-0.38	5.15	4.25	0.760	0.745	0.009
	P. depressa	0.32-0.33	WHOI	9.4	N/A	-0.36	5.13	4.23	0.803	0.788	0.015
	P. depressa	0.32-0.33	WHOI	9.4	N/A	-0.40	5.09	4.19	0.804	0.790	0.006
	P. depressa	0.32-0.33	WHOI	9.4	N/A	-0.33	5.17	4.27	0.777	0.763	0.011
	P. depressa	0.38-0.39	WHOI	10.7	N/A	0.34	5.00	4.10	0.814	0.799	0.014
	P. depressa	0.38-0.39	WHOI	10.7	N/A	0.33	5.06	4.16	0.789	0.775	0.012
	P. depressa	0.38-0.39	WHOI	10.7	N/A	0.35	5.10	4.20	0.792	0.778	0.009
	P. depressa	0.38-0.39	WHOI	10.7	N/A	0.36	5.06	4.16	0.777	0.763	0.013
Deglacial	P. depressa	0.47-0.48	WHOI	12.5	N/A	1.21	5.13	4.23	0.793	0.778	0.007
	P. depressa	0.47-0.48	WHOI	12.5	N/A	1.26	5.15	4.25	0.793	0.778	0.010
	P. depressa	0.47-0.48	WHOI	12.5	N/A	1.24	5.28	4.38	0.763	0.749	0.017
	P. depressa	0.53-0.55	WHOI	14.2	N/A	0.59	5.15	4.25	0.799	0.785	0.012
	P. depressa	0.53-0.55	WHOI	14.2	N/A	0.57	5.23	4.33	0.775	0.761	0.008
	P. depressa	0.53-0.55	WHOI	14.2	N/A	0.56	5.22	4.32	0.792	0.777	0.015
	P. depressa	0.59-0.62	WHOI	17.0	N/A	1.13	5.32	4.42	0.778	0.764	0.010
	P. depressa	0.59-0.62	WHOI	17.0	N/A	1.11	4.99	4.09	0.800	0.785	0.017

Glacial	P. depressa	0.67-0.68	WHOI	22.0	N/A	0.89	5.34	4.44	0.805	0.791	0.027
	P. depressa	0.67-0.68	WHOI	22.0	N/A	0.90	5.29	4.39	0.788	0.773	0.011
	P. depressa	0.68-0.69	WHOI	22.8	N/A	0.99	5.37	4.47	0.791	0.777	0.009
	P. depressa	0.68-0.69	WHOI	22.8	N/A	1.02	5.40	4.50	0.800	0.786	0.015
	P. depressa	0.69-0.70	WHOI	23.4	N/A	1.00	5.27	4.37	0.778	0.763	0.010
	P. depressa	0.69-0.70	WHOI	23.4	N/A	1.08	5.29	4.39	0.831	0.816	0.008
	P. depressa	0.69-0.70	WHOI	23.4	N/A	0.99	5.24	4.34	0.765	0.751	0.008
	P. depressa	0.71-0.74	WHOI	25.2	N/A	1.09	5.36	4.46	0.773	0.758	0.013
	P. depressa	0.71-0.74	WHOI	25.2	N/A	1.08	5.34	4.44	0.781	0.766	0.013
	P. depressa	0.71-0.74	WHOI	25.2	N/A	1.08	5.38	4.48	0.789	0.774	0.009
	P. depressa	0.76-0.77	WHOI	27.0	N/A	0.87	4.94	4.04	0.744	0.729	0.011
	P. depressa	0.76-0.77	WHOI	27.0	N/A	0.89	4.94	4.04	0.771	0.756	0.006
	P. depressa	0.76-0.77	WHOI	27.0	N/A	0.91	4.96	4.06	0.766	0.751	0.015
	P. depressa	0.76-0.77	WHOI	27.0	N/A	0.63	5.31	4.41	0.757	0.742	0.008
	P. depressa	0.77-0.78	WHOI	27.7	N/A	0.79	5.02	4.12	0.770	0.756	0.009
	P. depressa	0.77-0.78	WHOI	27.7	N/A	0.81	5.08	4.18	0.786	0.771	0.011
	P. depressa	0.77-0.78	WHOI	27.7	N/A	0.85	5.10	4.20	0.753	0.738	0.009
Holocene	P. depressa	0.20-0.21	ETH	6.9	5	-0.51	4.74	3.84	0.789	0.789	0.020
	P. depressa	0.20-0.21	ETH	6.9	10	-0.52	4.75	3.85	0.776	0.776	0.020
	C. wuell.	0.20-0.21	ETH	6.9	8	1.39	3.96	3.96	0.767	0.767	0.016
	C. wuell.	0.20-0.21	ETH	6.9	10	1.45	3.94	3.94	0.791	0.791	0.009
	C. wuell.	0.20-0.21	ETH	6.9	6	1.42	3.90	3.90	0.787	0.787	0.015
	P. depressa	0.28-0.29	ETH	8.5	7	-0.40	4.88	3.98	0.757	0.757	0.011
	P. depressa	0.28-0.29	ETH	8.5	3	-0.39	4.95	4.05	0.799	0.799	0.020
	P. depressa	0.28-0.29	ETH	8.5	10	-0.40	4.91	4.01	0.771	0.771	0.008
	P. depressa	0.28-0.29	ETH	8.5	14	-0.04	5.02	4.12	0.784	0.784	0.009
	P. depressa	0.28-0.29	ETH	8.5	14	-0.38	4.94	4.04	0.761	0.761	0.008
	C. wuell.	0.32-0.33	ETH	9.4	9	1.24	4.12	4.12	0.762	0.762	0.011
	C. wuell.	0.32-0.33	ETH	9.4	5	1.23	4.20	4.20	0.796	0.796	0.010
	C. wuell.	0.32-0.33	ETH	9.4	8	1.32	4.28	4.28	0.814	0.814	0.014
	P. depressa	0.32-0.33	ETH	9.4	5	-0.34	5.04	4.14	0.783	0.783	0.019
	P. depressa	0.32-0.33	ETH	9.4	5	-0.31	5.12	4.22	0.755	0.755	0.015
	P. depressa	0.38-0.39	ETH	10.7	2	0.42	4.98	4.08	0.759	0.759	0.033
	P. depressa	0.38-0.39	ETH	10.7	12	0.37	5.03	4.13	0.767	0.767	0.010
	P. depressa	0.38-0.39	ETH	10.7	7	0.37	4.97	4.07	0.741	0.741	0.011
Deglacial	P. depressa	0.47-0.48	ETH	12.5	8	1.20	5.03	4.13	0.764	0.764	0.009
	P. depressa	0.47-0.48	ETH	12.5	9	1.18	5.04	4.14	0.749	0.749	0.012
	P. depressa	0.47-0.48	ETH	12.5	9	1.18	5.04	4.14	0.769	0.769	0.006
	P. depressa	0.53-0.55	ETH	14.2	8	0.57	5.04	4.14	0.763	0.763	0.010
	P. depressa	0.53-0.55	ETH	14.2	6	0.63	5.08	4.18	0.760	0.760	0.007
	C. wuell.	0.55-0.57	ETH	15.0	9	1.02	3.28	3.28	0.771	0.771	0.016
Glacial	P. depressa	0.64-0.67	ETH	20.8	4	1.05	5.08	4.18	0.796	0.796	0.022
	P. depressa	0.64-0.67	ETH	20.8	10	1.32	5.32	4.42	0.738	0.738	0.010

P. depressa	0.67-0.68	ETH	22.0	8	0.72	5.07	4.17	0.749	0.749	0.009
P. depressa	0.68-0.69	ETH	22.8	7	0.98	5.32	4.42	0.750	0.750	0.012
P. depressa	0.68-0.69	ETH	22.8	7	1.04	5.44	4.54	0.767	0.767	0.015
P. depressa	0.69-0.70	ETH	23.4	9	0.93	5.05	4.15	0.772	0.772	0.011
P. depressa	0.70-0.71	ETH	24.0	12	1.03	4.95	4.05	0.764	0.764	0.011
P. depressa	0.71-0.74	ETH	25.2	10	0.97	5.10	4.20	0.775	0.775	0.006
P. depressa	0.71-0.74	ETH	25.2	8	1.19	5.35	4.45	0.768	0.768	0.009

Table S4. Clumped isotope data summary from the two laboratories

	Mean Holocene Δ_{47}	Mean Glacial Δ_{47}
WHOI with -0.0145 ă offset	0.773±0.004ă	0.765±0.006ă
WHOI with no offset	0.788±0.003ă	0.779±0.005ă
ETH	0.775±0.004ă	0.764±0.006ă
Combined (using offset WHOI)	0.774±0.003ă	0.765±0.004ă

Table S5. *C. wullerstorfi* (Cw), *N. pachyderma sinistral* (Nps) stable isotopes, and *O. umbonatus* (Ou) stable isotopes and Mg/Ca-inferred bottom water temperatures for core MD992276.

Depth (cm)	Age (ka)	Nps $\delta^{18}O$ (‰)	Cw $\delta^{13}C$ (‰)	Cw $\delta^{18}O$ (‰)	Ou $\delta^{18}O$ (‰)	Ou $\delta^{13}C$ (‰)	Ou Mg/Ca (mmol./mol.)	Temperature (^{o}C)
94	11.9	3.89	N/A	N/A	N/A	N/A	N/A	N/A
95	11.95	3.93	N/A	N/A	N/A	N/A	N/A	N/A
96	12.00	4.35	1.31	3.86	N/A	N/A	1.33	-1.43
97	12.20	3.86	1.37	3.99	4.57	-1.26	1.28	-1.75
98	12.40	4.36	1.26	3.90	4.67	-1.31	1.33	-1.37
99	12.60	4.53	1.42	3.77	4.55	-1.22	1.31	-1.59
100	12.80	4.51	1.16	3.84	4.52	-1.21	1.38	-1.05
101	13.00	4.44	1.24	3.90	4.55	-1.29	1.34	-1.34
102	13.20	4.5	1.33	3.81	4.67	-1.40	1.36	-1.13
103	13.40	4.39	1.20	4.04	4.56	-1.27	1.35	-1.24
104	13.60	4.6	1.39	4.02	4.65	-1.34	1.27	-1.89
105	13.80	4.19	1.33	3.93	4.56	-1.37	1.23	-2.14
106	N/A	4.38	N/A	N/A	N/A	N/A	N/A	N/A
107	14.20	4.32	1.44	3.78	N/A	N/A	1.30	-1.62
108	14.40	4.19	0.81	3.58	4.60	-1.57	1.33	-1.41
109	14.67	4.04	0.99	3.55	4.56	-1.50	1.31	-1.58
110	14.94	3.93	1.11	3.69	4.43	-1.53	N/A	N/A
111	15.21	3.47	0.83	3.27	4.52	-1.72	1.32	-1.52
112	15.48	3.72	0.78	3.23	4.42	-1.65	1.33	-1.41
113	15.75	4.02	0.76	3.34	4.43	-1.60	1.39	-0.96
114	16.02	3.73	0.86	3.31	4.42	-1.68	1.48	-0.28
115	16.29	3.81	0.99	3.37	4.46	-1.64	1.39	-0.98
116	16.56	4.24	0.93	3.45	4.42	-1.71	1.41	-0.76
117	16.84	4.47	1.04	3.46	4.54	-1.63	N/A	N/A
118	17.11	4.45	1.07	3.61	4.59	-1.67	1.44	-0.56
119	17.38	4.77	0.77	3.28	N/A	N/A	N/A	N/A
120	17.65	4.86	1.28	3.79	4.74	-1.88	1.69	1.36
121	17.92	4.79	1.27	3.86	4.73	-2.08	N/A	N/A
122	18.19	4.79	1.26	4.00	N/A	N/A	N/A	N/A
123	18.46	4.77	1.22	3.68	N/A	N/A	1.71	1.50
124	18.73	4.9	1.04	3.61	N/A	N/A	N/A	N/A
125	19.00	4.9	1.36	3.74	N/A	N/A	N/A	N/A